Sensory dependencies rapidly and autonomously yield generalizable representations in recurrent cortical-like networks

Udaya B. Rongala[1] and Henrik Jörntell[1]

[1] *Neural Basis of Sensorimotor Control, Department of Experimental Medical Science, Lund University, Lund, Sweden*

correspondence e-mail: udaya_bhaskar.rongala@med.lu.se, henrik.jorntell@med.lu.se

Abstract

How biological brains become operational so quickly is an unresolved issue. Here we evaluate the emerging effects in a fully recurrent network model that learns from simulated real-world interactions translated into spatiotemporal sensory input patterns via a model tissue with intrinsic biomechanical dependencies. We used local Hebbian plasticity rules and continuous random mechanical activations of a mass-spring-damper model of skin tissue, thereby mimicking the process of early brain development observed in humans and animals alike. The recurrent network, emulating a generic, primitive cortical-like subnetwork, was composed of fully connected excitatory and inhibitory neurons, with independent learning in both types of synapses. Continual random external activations of the skin, without resetting the network state, led to rapid acquisition of remarkably robust and generalizable representations of the skin inputs. The trained network could separate various dynamic skin inputs and solve a kinematics task it had never encountered, even when substantial parts of the sensor population or internal network connections were removed post-training. Hence, random exploration rapidly led to network representations of the dominant tissue dynamics, equaling emergent predictive coding that was applicable to separate diverse mechanical real-world interactions.

A striking difference between biology and artificial intelligence is that the brain seems to be learning effectively from much fewer examples and much less repetitious inputs (1). Why that happens is an unresolved issue that could have wide repercussions on holistic views of the purpose of learning in the brain. We hypothesized that one reason could be that the brain learns about the world through the lens of the biomechanical properties of its body. The body is composed of tissues with dynamic compliances, such as in the skin (2) but also in deep tissues in general, which essentially make the whole body mechanically coupled (3). A system with many components where those components interact with each other with linkages at various spatial and temporal scales is a definition of *complexity* in system theory. The biological body can be considered to have evolved with respect to functional complexity, in order to increase the variety of actions the organism is capable of (4). Because the sensors are distributed within such compliant tissues they can display complex patterns of dependencies, which can be quantified by the entropy in the sensor population signal (2). It is important to note that despite the increased complexity, mechanical couplings will inevitably create dependencies and result in various spatiotemporal regularities in the sensor population signals. Combining information expressed on the basis of such regularities could be used to represent in principle any conceivable event by means of the principle of superposition (2, 5, 6, 7, 8). A network learning strategy that focuses

on representing such regularities as broadly as possible would in turn become more generalizable (7) and more robust to sensor loss and/or sensor drift as well as localized brain damage, which would be valuable features in biological life and evolution.

We tested the general principles of this postulate by studying learning on sensor inputs, which were generated by a spring-mass-damper model of skin tissue dynamics (2), in a fully connected recurrent neuronal network. Our aim was to study emergent effects in the simplest possible network that would still be capturing central functional principles compatible with a primitive cortical circuitry, for example early in development or early in evolution (9, 10, 11). In general, networks with extensive recurrent connections, similar to Reservoir Computing (RC) or Echo State (ESN) networks, have been taken as reflective of the general principles of cortical network operation (12, 13) (in contrast, the networks in the brainstem nuclei and the cerebellum, for example, have less of recursive connectivity and are more feed-forward in character (8, 14)). Similarly, we were here more interested in features conveying overarching functional effects rather than copying the histological structure of the cortex. There are plenty of biological motivations for the network architecture we employed, which we provide in the Methods. Naturally, in its mature state the cortical network is not fully connected but the rules deciding which connections are supported are not known and we chose to keep the network fully connected and instead let the emerging functionality of the network decide which connections should be reduced.

We used training on random sequences of non-repetitious activations of the skin model, where the sensors had extensive intrinsic dependencies (2), and we find that the network learned to separate a diversity of previously unseen spatiotemporal inputs (naive inputs). The network could also separate different kinematics of given naive inputs. Ablation experiments after completed training showed that the network performance was still almost unaffected when parts of the sensor population or substantial parts of the network-internal connections were removed. Comparisons with the pre-training network across noise levels indicated that the training caused the network to better mirror at least some of the diverse dynamics of the sensor data from the skin model. Although with a number of caveats, our results indicate that sensors with intrinsic dependencies along with simple learning rules can result in emergent learning effects, similar to those observed in early development and infants (15, 16). These emergent effects can quickly make the network operational by achieving initial, generalizable 'good enough' solutions to intrinsically complex high-dimensional dynamic sensor inputs.

Results

Network learning from intrinsic dependencies

Fig. 1A illustrates the fully connected network that comprised both excitatory and inhibitory neurons. Most of the experiments in this paper was done on the '5 × 4 x 2' network architecture, with five ENs and five INs in layer 1 and four ENs and four INs in layer 2, fir a total of 18 neurons. These networks were trained to study the impact of sensory inputs with and without intrinsic dependencies, using Hebbian-like plasticity across all synapses. Fig. 1B illustrates the mass-spring-damper model of biologically measured skin dynamics (2), with extensive resulting codepencies between the sensors. Fig. 1C shows one example skin input alongside one example Gaussian input, the latter being devoid of intrinsic dependencies and used as the control training input. The temporal profiles of the skin sensor responses illustrated that each sensor provided non-redundant information due to the distributed dynamic couplings, i.e. the springs.

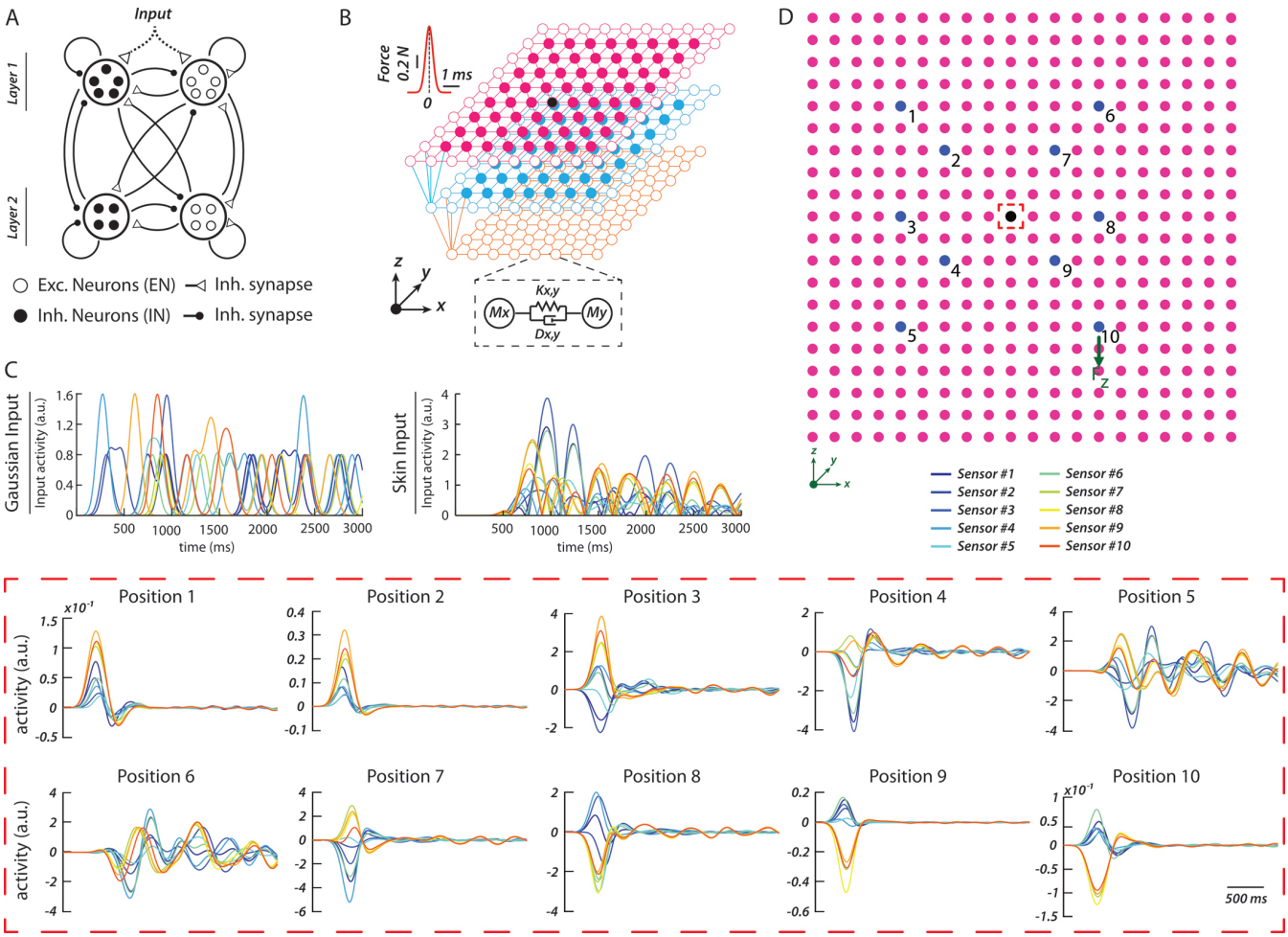

Figure 1: **Network structure and training inputs from the dynamic skin tissue model** (**A**) Schematic of the fully connected network structure. (**B**) Three-layer damped mass-spring skin model (2) used to generate the intrinsically dependent sensory inputs. Top left corner, time profile of the applied forces for the different inputs. Masses, shown as nodes, were connected by springs and dampers represented as links (internode distance 1.0 mm). Note that the actual model was larger and comprised 1085 nodes in total. Nodes shown as circles along the edges were fixed nodes, including the entire third layer. The activity from the 10 sensors connecting to the mass at the center of the superficial layer (black node) were provided as input to the network. (**C**) Example sensory inputs used for network learning. One diagram illustrates the 10 sensor inputs for a Gaussian input, the other diagram illustrates the 10 sensor inputs for a skin input. (**D**) The 10 input locations used to apply the skin inputs are indicated on the first layer of the skin model, relative to the location of the central mass (black). Red dashed box below illustrates the skin sensor responses from the 10 springs attached to the central mass, and used as the training inputs, when one of the training inputs, Input #1 (Indent, Fig. S1), was applied to the different input locations (nodes colored in blue). The activity of all skin sensor signals were made to be positive-only by rectification. As an example, the skin input in panel C is the rectified skin input evoked from Position 5.

As the actions driving the early learning in biological brains are far from structured ('*motor babbling*'; see (16, 17)), our network training consisted of a series of random, non-repetitive activations of the skin model, in what would correspond to less than one hour of random haptic interaction in a biological system. We implemented randomness in the learning process by using a varied set of spatiotemporal force input patterns (Fig. S1) and by that every subsequent input was delivered to a random location on the skin (Fig. 1D). Because of the small size of the network, only the 10 sensors connected to the central mass (indicated in black in Fig. 1B, D) were providing input to the network, and their responses varied greatly depending on input location (Fig. 1D). Note that biological skin has a lower sensor density than what our skin model can allow for (2) and such sensory subsampling, which was hence also reflected in our setup, would tend to bias the network to learn the dominant dependencies within the skin

model. The continual nature of the activations also meant that the circulating activity within the recurrent network was never allowed to fully relax between consecutive stimuli. Hence, each stimulus presentation was met with a potentially unique processing state in the network (18), rendering each learning phase even more unique. To test the impact of the intrinsic dependencies across the sensor population, we compared the learning obtained from skin inputs with the learning obtained in the same initial network instead trained on the pre-generated random patterns of Gaussian signals ('Gaussian network') (Fig. 2). The Gaussian signals were generated in such a way that they matched the overall frequency and power distribution of the skin inputs (Fig. S2). Figure 2 illustrates the neuron activities comprehensively as well as in detailed snapshots, pre-(red arrows) and post-(green arrows) learning, for the 'skin network' as well as for the 'Gaussian network'. On visual inspection, the neuron signals became more structured in the skin network compared to the Gaussian network (Fig. 2 C, D).

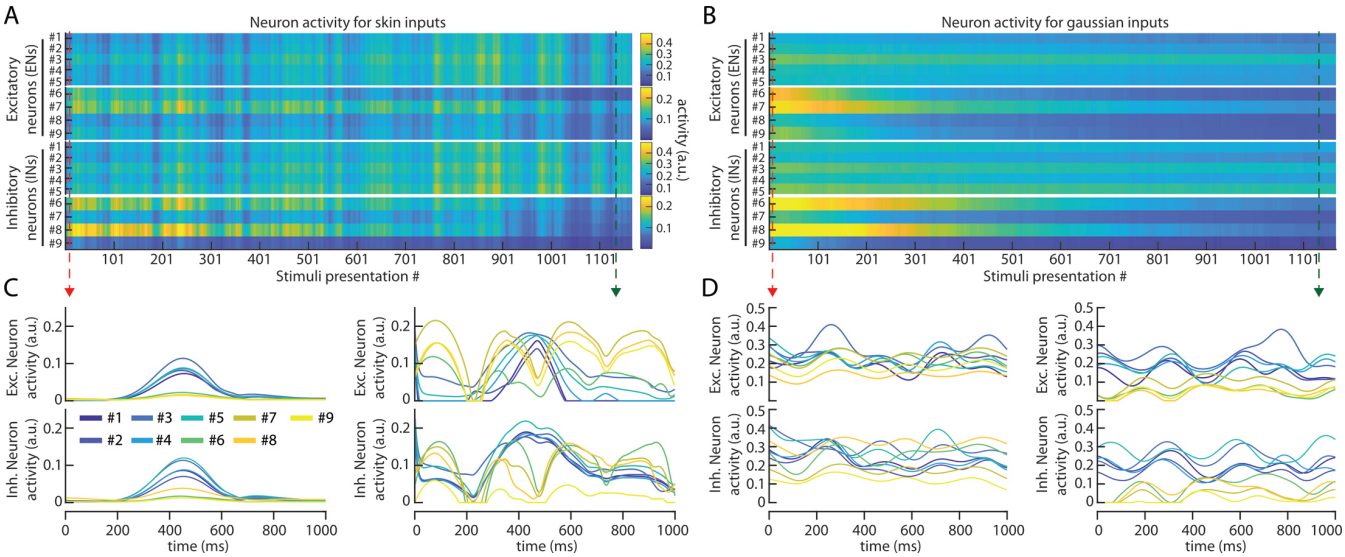

Figure 2: **Network learning from skin and Gaussian inputs** (**A**) Individual neuron activities (moving average across 50 input presentations) during learning from an uninterrupted sequence of 1160 random skin inputs. This network had initial connectivity%=23. (**B**) Corresponding network learning from the Gaussian inputs. (**C**) Activities of the excitatory (top) and inhibitory (bottom) neurons (N=9 neurons per group, blue neurons were located in layer 1) to an example skin input at the beginning (left) and at the end (right) of the learning. (**D**) Similar display for a Gaussian input.

Separation of naive inputs

A critical research question was if learning on the signals with the intrinsic dependencies (skin network) could cause an improved generalization in the network. Generalization could be demonstrated as a capacity to separate inputs that the network had not previously experienced during the training ('naive inputs'). To address this question, we analyzed the activity distribution patterns across the neuron population using principal component analysis (PCA) (i.e. quantifying any regularities in the network activity arising as a consequence of learning). Post-learning skin networks and Gaussian networks (Fig. 3A) were provided with naive skin inputs (Fig. 3B), which differed either with respect to their spatial force pattern (input type) (Fig. S1) or they consisted of different temporal profiles (kinematics) of force impulses with a simple spatial structure (Fig. S3).

For the five naive skin inputs, the skin networks provided more distinctly different neuron population activity trajectories in the PC space than the Gaussian networks (Fig. 3C; Fig. S4 illustrates the PC trajectories for the untrained, random network). Using five different initial network configurations (each with the same initial connec-

tivity% of 23%, see section 'Synaptic weight changes') and testing them across a range of different neuronal noise levels, we found that the skin networks (in comparison to Gaussian and pre-learning networks) provided a lower classification error rate across the different naive skin inputs (Fig. 3D). The classification error rate was relatively consistent across all the different initial network settings (referred to as 'Initial Connectivity%,'Fig. S5). When we next tested the performance of the networks for the separation of force impulses with different kinematics (Fig. S3), which the networks had not been trained on, there was an even clearer separation between the two network types (Fig. 3E,F).

Notably, across all tests, the skin network, unlike the Gaussian network, outperformed the pre-learning network, except at the lowest noise levels, where the networks approached deterministic behavior. The fact that even the untrained, random network could separate inputs during deterministic operation is in line with the known behavior of RC or ESN networks. Because even random recursive networks have default intrinsic dynamic modes, they can provide for some level of separation capacity for dynamic inputs (19). However, neurons in the brain *in vivo* do not operate without noise (20, 21) and hence we believe our higher noise levels are more reflective of what biological neuronal networks can achieve in terms of input separation. The fact that the skin networks performed progressively better compared to the pre-learning network with increasing noise levels (Fig. 3D,F) indicates that learning on intrinsic dependencies led to representations that focused on the dominant dynamics of the sensor inputs. Hence, learning on inputs with intrinsic dependencies between sensors led to an improvement in the generalized separation capacity of the network, whereas training on inputs without such sensor dependencies could even lead to a performance loss compared to the randomly connected pre-learning network.

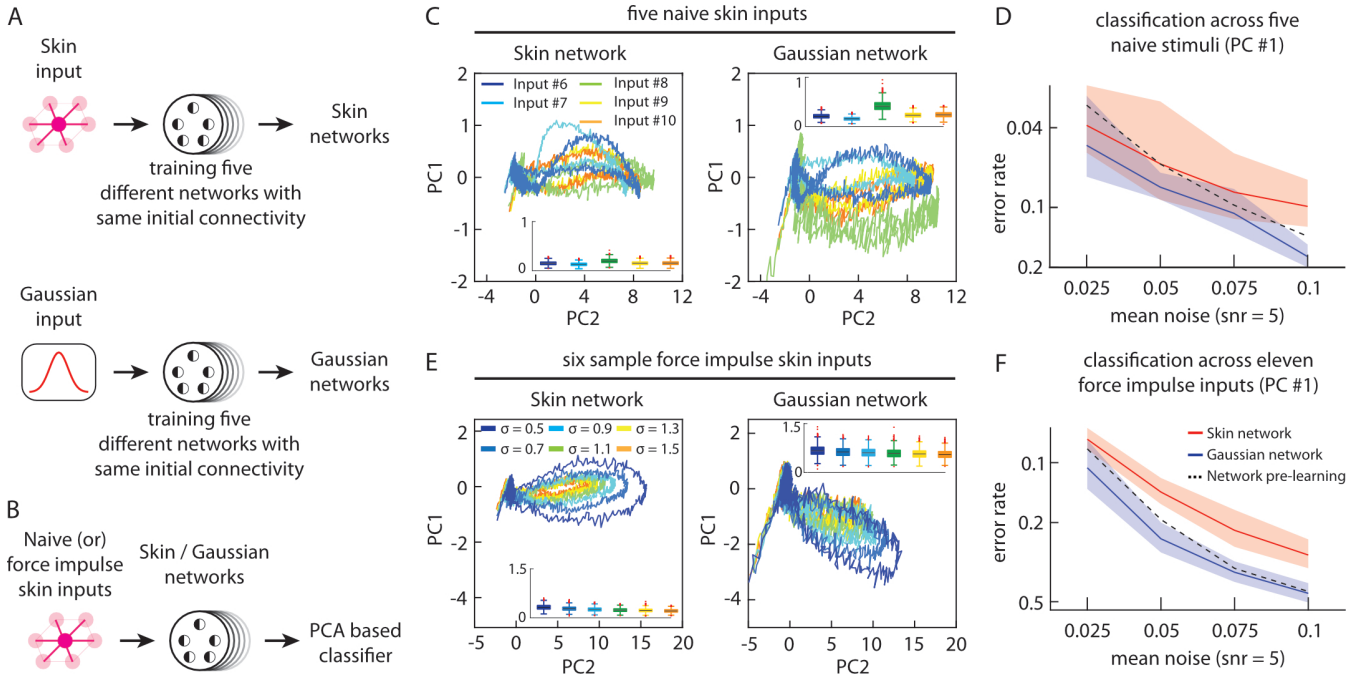

Figure 3: **Generalization to naive skin inputs** (**A**) The network learned from skin inputs or from Gaussian inputs. (**B**) Protocols used for comparing the classification generalization. (**C**) The responses of the excitatory neuron population for the five naive skin inputs Fig. S1 F-J; color coded) projected on the first two principal components (PCs), comparing the skin and Gaussian networks (at a neuronal noise level of 0.1). *Inset*: the variances of the PC scores for the five different inputs. Same network as in Fig. 2. (**D**) Classification accuracies (mean and variance) across the five naive skin inputs at different noise levels. (**E**) Similar display as in **C**, but for eleven force impulse skin inputs (Fig. S3). (**F**) Classification accuracy across these eleven force impulse skin inputs.

Network Scaling

Most of the work in this study used a '5 × 4 x 2' network architecture with a total of 18 neurons (Fig. 1A), but we also tested how scaling the network size affected the classification of the naive skin inputs. When increasing the number of neurons in each layer, we kept the same connectivity rules for internal and external inputs. The performance improved slightly in larger networks, which could in part be due to that the higher number of neurons cause a better noise averaging effect.

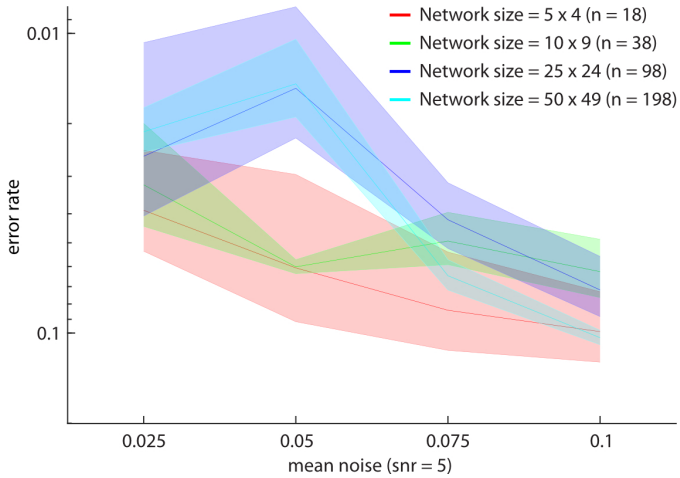

Figure 4: **Network size.** Skin network classification accuracies (mean and variance) across the five naive skin inputs at different noise levels, for four different network sizes. 'n' indicate the number of neurons for the two layers, for either the excitatory or the inhibitory neurons (hence, the largest network, 50 x 49 x 2, had a total of 198 neurons).

Robustness

We also tested the impact of removing sensors and internal synapses post-learning (Fig. 5). Despite removal of 20% of the sensors, the PC trajectories did not substantially alter (Fig. S6) and the classification for both naive and force impulse skin inputs was unchanged or improved for the skin network, in contrast to the Gaussian network (Fig. 5A). Perhaps even more remarkable, the skin networks were highly robust to removal of network-internal synapses, and even when 75% were removed the network separation of the naive skin inputs was still not degraded (Fig. 5B). This indicates that the training on the skin inputs resulted in systematic changes in the network structure, likely causing its internal activity dynamics to become entrained to the underlying sensory dependencies, making the representations broad-based and therefore incredibly robust. This would be conferring robustness to damages to the body, or to the brain (22), which would have major survival value. Note that, similar to (Fig. 3D,F), the performance of the skin network progressively improved relative to the pre-learning network with increasing noise levels, indicating that the skin network had a better approximation of the dependencies within the skin inputs.

Learning on the Gaussian input did also in this case reduce the separation capacity of the pre-learning network (Fig. 5). This suggests that training on the Gaussian inputs altered the synaptic weights in such a way that the network activity became harmonized with its own internal dynamics, thereby possibly shutting itself off from being impacted by the sensory inputs. When the ablation level increased, the difference between Gaussian and pre-training networks was eventually lost (Fig. 5B). This makes sense if the Gaussian input could not create any deep structural changes to the network due to the absence of intrinsic dependencies.

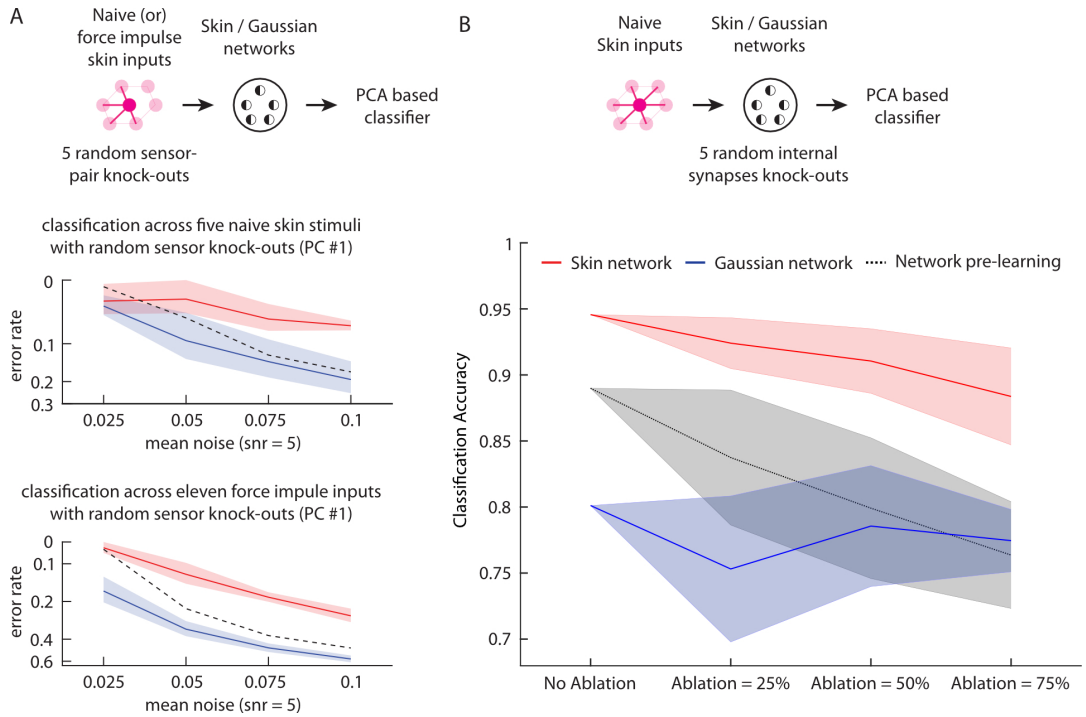

Figure 5: **Ablation of random subsets of sensors or internal connections post-learning.** (**A**) Protocol used for comparing the classification robustness with random sensory knock-outs. (**bottom**) Classification accuracies (mean and variance) across the five naive skin inputs and eleven force impulse skin inputs with random sensory knock-outs, at different noise levels. (**B**) Protocol used for comparing the classification robustness with network ablation. (**bottom**) Classification accuracies (mean and variance) across the five naive skin inputs, for three different levels of network internal synapse ablation. In the ablation study, 2, 4, and 6 randomly selected internal synapses per each neuron were removed from the network to simulate 25%, 50%, and 75% ablation levels, respectively.

Synaptic weight changes

Relative to the pre-learning network (Fig. 6A-C), training on skin inputs caused an increase in the weights of the sensory synapses (red dotted box, Fig. 6A), whereas the opposite effect applied to the Gaussian network (Fig. 6D; note the scale difference for the two networks). There were also extensive reorganization and excitatory/inhibitory re-balancing of the network internal synapses (Fig. 6E), which gradually stabilized during the course of the training for both skin (Fig. S7, S9) and Gaussian networks (Fig. S8). This reorganization can explain how the skin network activity could decrease (Fig. 2A,B) when its synaptic weights increased.

To test the learning across a variety of initial network connectivities, we used 30 different network settings, each fully connected, identified by their 'Initial connectivity%'. This label reflected the mean weights of the synapses but was also an index indicating the weight distribution (see Fig. S11, S12) and weight skewness (Fig. S13). The initial network activity scaled roughly linearly with the 'Initial connectivity%'s (Fig. S10). Whereas the sensory synapses overall changed the most, the internal network synapses could change almost as much for the networks with intermediate Initial connectivity% (20-35%) (Fig. 6F-I), in particular the feedback connections from layer 2 to layer 1 (Fig. S14). Further, the weight changes of the internal synapses on the excitatory and inhibitory neurons were similar across the different Initial connectivity%'s for the two network types (skin and Gaussian) (Fig. 6G,I). The skewness of the initial weights generally increased by the Initial connectivity% value (Fig. S13), but did not have any apparent relationship to these weight changes (Fig. S15).

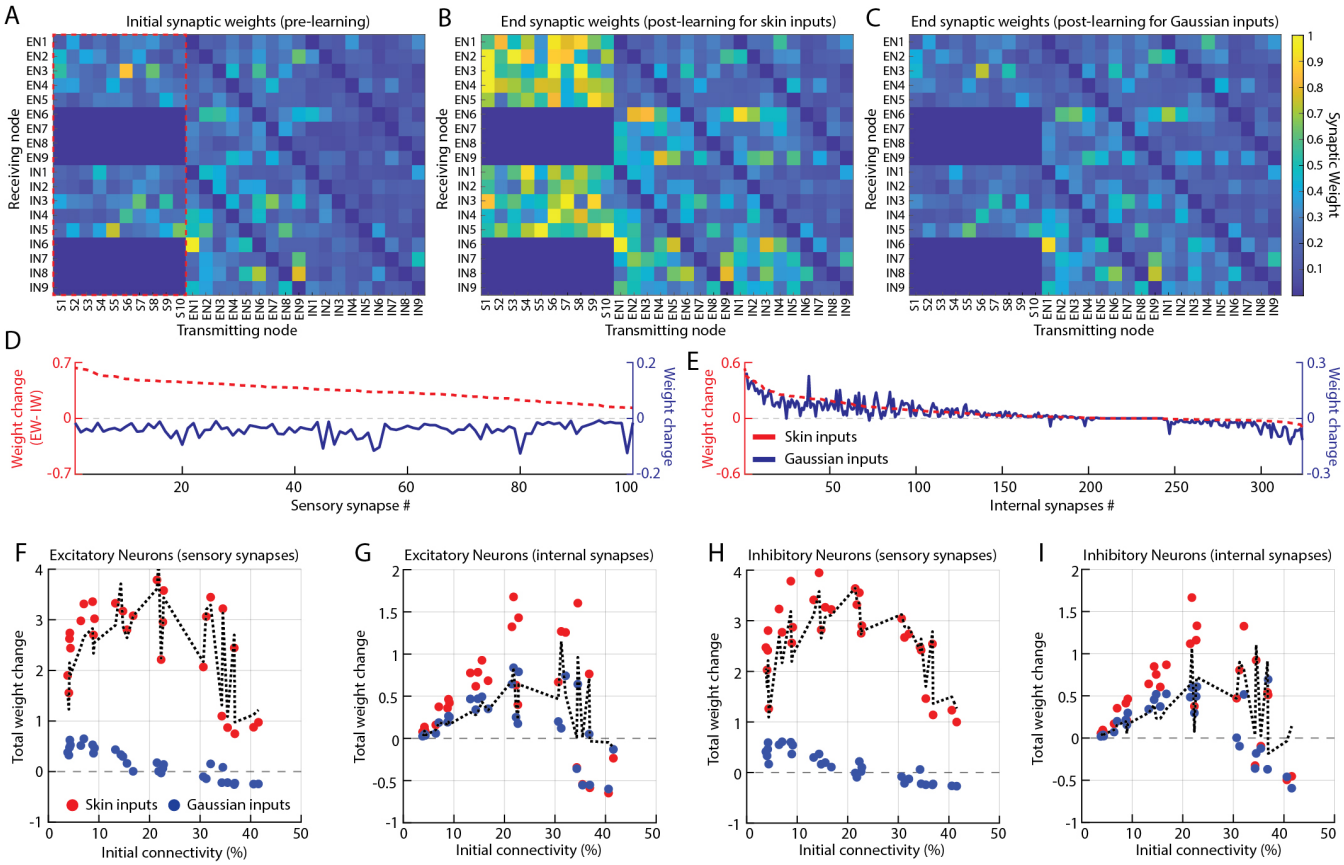

Figure 6: **Synaptic weight changes following learning** (**A**) Initial synaptic weights for an example network (same network as in Fig. 1.) with the sensory synapses within the red dotted box. (**B**) The synaptic weights post-learning (end Weights) in the skin network. (**C**) The synaptic weights post-learning in the Gaussian network. (**D**) Sensory synapses sorted by their magnitude of weight change after learning from the skin input, for comparison of the skin network and the corresponding Gaussian network. (**E**) Similar display as in **D**, but for weight changes across non-sensory synapses (internal synapses). (**F-I**) Average net weight changes post-learning, sorted by type of synapse, across networks with varied initial weight configuration (Fig. S11, S12). The dashed lines indicate the difference in average net weight changes between the corresponding skin networks and the Gaussian networks.

The effect of response differentiation across the neurons

We observed that the cross-correlation measure of the activity between the neurons decreased substantially with learning in the skin networks (Fig. 7A,B). However, for the networks with the highest connectivity% such a drop did not occur. These networks also had the lowest degree of restructuring of their synaptic weights (Fig. 6F-I). We hypothesized that the internal activity in these tight networks were too strong for their weights to become sufficiently impacted by the sensory synaptic activities. We investigated if a drop in the cross-correlation in these cases could be 'rescued' by a tweak to the learning rule such that the excitatory synapses were only allowed to 'see' a high pass filtered version of the postsynaptic signal used for learning. Implementing this 'Excitatory synapse learning signal filter' led to drops in the cross-correlations within the networks with high initial connectivity%, with much lower impact on the networks with the lowest initial connectivity% (Fig. 7C, Fig. S16). Also the overall pattern of synaptic weight changes remained unchanged (compare Fig. S17 with Fig. 6F-I). Importantly, for the networks with high initial connectivity%, the learning signal filter did indeed also lead to a 'rescue' of their input separation capability (Fig. 7D); the filter reduced the classification error rate from 0.12 (left) to 0.01 (right)).

Finally, removing inhibitory synapses, both laterally within the layers and feed-forward connections, led to

significantly higher cross-correlations after learning, whereas removing other connection types one-by-one did not have a consistent impact (Fig. S18). Hence these inhibitory connections could be more important for the network to acquire a high separation capacity.

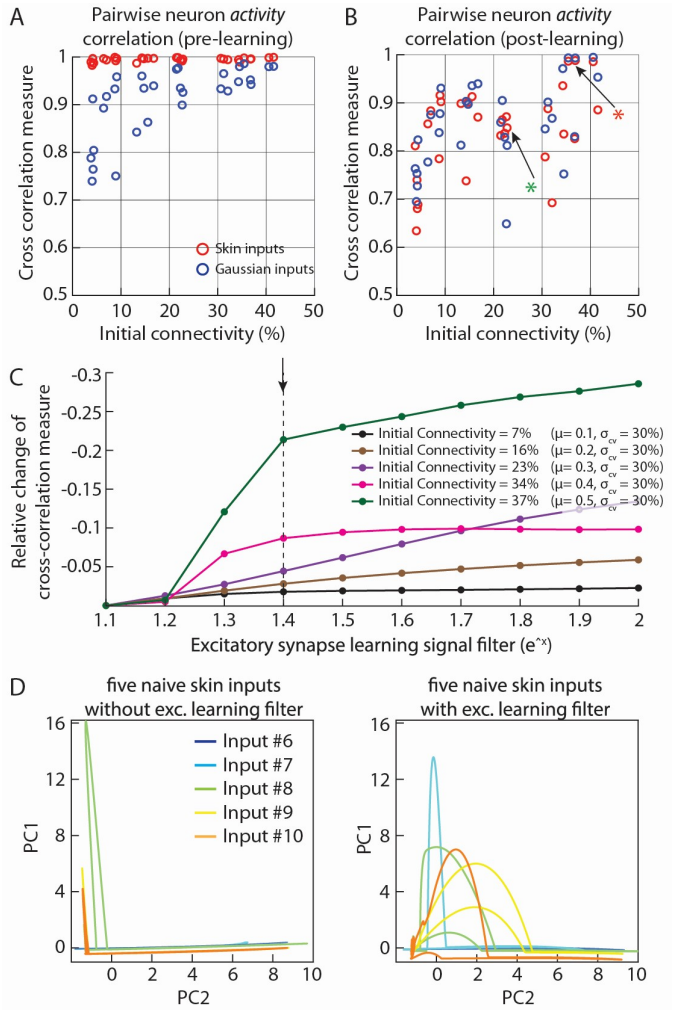

Figure 7: **Diversification of the neuronal activity post-learning and 'rescue' effect of the excitatory learning signal filter.**(**A**) Average pairwise cross-correlations across all the ENs pre-learning. (**B**) Same observation post-learning. Arrow with *green asterisk* indicate the network illustrated in Figs 2, 3 and the arrow with *red asterisk* indicate the network that failed to learn without learning signal filter. (**C**) Relative changes in the cross correlation measure in skin networks across different learning signal filter exponents. Dashed line indicates the exponent (1.4) used in the test in (D). (**D**) PC trajectories of the failing post-learning network without the learning signal filter (left) and the same network with the learning signal filter (right).

Discussion

We illustrated the emergent effects of Hebbian-like learning in a fully recurrent neuronal network when the sensory inputs have intrinsic dependencies. The learning featured non-repetitive spatiotemporal inputs, compatible with early biological development, which is characterized by mostly disorganized, semi-chaotic movements and real-world interactions (15, 16, 23, 24), and was independently controlled by each individual excitatory and inhibitory synapse. We found this learning strategy to quickly converge towards highly generalizable network representations, applicable to separate novel inputs from the same sensorized system with diverse spatial and/or kinematic char-

acteristics. The network representations were also remarkably robust to post-learning loss of sensors and internal connectivity, in addition to neuronal noise. The model responses to the spatiotemporal sensor input patterns in principle resembled those of cortical neurons *in vivo*, which depend on various time-varying dynamics of recurrent connections that gradually unfold during the course of spatiotemporal sensory inputs (18, 25, 26).

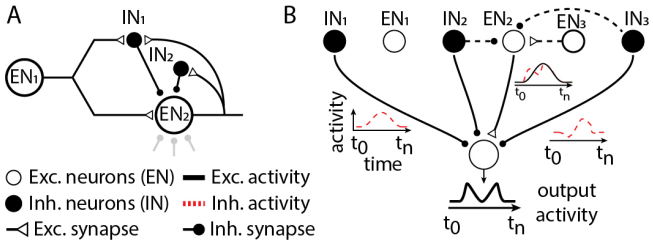

Figure 8: **Diverse effects of synaptic inhibition in recurrent networks.** (**A**) Scenario when feed-forward inhibition and feedback inhibition are mediated by the same inhibitory interneuron. Lower part, if multiple inhibitory interneurons provide input to EN_2 (shaded synapses below EN_2), the inhibitory control can sometimes have the properties of 'detailed' inhibition, and sometimes have the property of 'blanket' or 'global' inhibition (see text). (**B**) A feed-forward excitatory pathway via EN_2 would lose its signal if the inhibitory signal was identical. A more diversified set of inhibitory signals (red traces) will transform and thus propagate parts of the excitatory signal (black traces).

What was the nature of the emergent network representations?

Since the sensory inputs were generated via a skin model with intrinsic dependencies, the recursive network was forced to learn the dominant skin dynamics (encoded in the sensory co-dependency patterns (2)) across diverse mechanical inputs, as there was essentially nothing else for it to learn. In this setting, when the incoming sensory information combines with the ongoing recurrent network activity this leads to a dynamic transformation of the sensory input within the network (cf. Fig. 1 and Fig. 2), rather than a straight-forward one-to-one mapping between the inputs and the corresponding output of the network. Focusing on learning to approximate the dominant regularities in the sensory data, as previously observed in neurons of the cuneate nucleus *in vivo* (6, 8), would make sense if the evolutionary pressure on the cortex is to become operational early in development and then gradually improve its capacity of transforming sensory information across temporal and spatial scales to continually update behavior.

We showed that the network tended to learn the dominant dynamic behaviors of the skin model through the conserved capacity to separate the skin inputs when internal connections or sensors were removed after learning (Fig. 5A,B); and when increasing noise levels in the network led to that the skin network became increasingly better than the pre-learning networks (Fig. 3,5). The same learning protocol, but without the sensory dependencies ('Gaussian networks'), instead even degraded the network performance. Since the dependencies across the sensors derive from the mechanical couplings in the tissue, which will impose a tissue-specific transformation on the sensory representation of any real world interaction, a similar set of dependencies would in principle be present across any stimulus/activation context. This effect could thus be used by the network to separate real-world interactions, even when they have not been previously experienced, by the principle of superposition of its representations of those dependencies. The aspects of the sensory dependencies in concert with the network internal dynamics should be the most easily learnt (in line with recent observations from early development (27, 11)). Notably, when the network begins to mirror the dynamics in the mechanical system, this is equivalent to the network beginning to predict or anticipate those dynamics (19). Hence, this learning strategy tends to emerge into predictive coding, which is widely held to be an important mode of operation in the cortex (28, 29).

Relationship to models of brain operation

The emergent network representations of this learning strategy aligns well with that most animals need to quickly learn to cooperate with the embedded dynamics in their body, because utilizing such *embodied intelligence* can lead to large gains in terms of control effort (3, 30, 31) and thereby shorten the time until the brain networks become operational. From an evolutionary point of view, it can be argued that increasing body complexity emerged from the need to increase the variety of actions in order to cope with more diverse environmental perturbations (4). We believe that in order to utilize those advantages, one task of the brain will then be to learn how to best mirror the dependencies that inevitably exists in that complex system, i.e. in principle to approximate its diverse dynamics to be able to find 'good enough' sensorimotor transformations (32) across contexts. To evaluate our networks in this regard we used PCA of the neuron population activity to quantify its emerging regularities, which is considered a well-suited analysis in the domain of complex systems (4), despite its limitations in identifying the important temporal dependencies of those regularities. In this model of brain operation, the focus on a gradual emergence of 'good enough' approximations of the dynamics in embodied intelligence could explain why the brain can become operational so quickly but also why random explorative learning leads to a gradually improving control, as it does in infants (15). Notably, the network size would hence not alter the computational architecture *per se* but it would increase its capability to approximate the dependencies (Fig. 4) in a scalable manner.

The importance of neuronal decorrelation for the separation capacity

The quantification of the input separation relied on differences in the time series of activity distributions across the neuron population (Fig. 3), ultimately also the defining basis of behavior (33). Decorrelation between the neurons can be a proxy for the input separation of the network (6, 34, 35) and cortical neuron populations display a great degree of decorrelation across various conditions (26, 34, 36, 37). In recurrent variational autoencoders, a type of artificial neural network, enforcing decorrelation during the learning of dynamic control tasks leads to more efficient representations (38). In our networks, the simultaneous excitatory and inhibitory synaptic plasticity would in principle lead to the inhibition canceling out the excitation, but as the sensory input is excitatory, inhibition will always be lagging 'one step behind', leaving some net excitation to induce decorrelation between the neurons (Fig. 8, S18). In the networks with higher connectivity% decorrelation did not evolve to the same extent, but was 'rescued' by the learning signal filter which also improved the input separation (Fig. 7). In biological neurons, the learning signal filter could be that the dendritic spines, receiving excitatory synapses (39), differentiates the calcium signal available to the postsynaptic enzymatic machinery controlling the synaptic weights (8) or simply synapse-dependent differences in that machinery. Experimental measurements of the biological fine tuning of the excitatory and inhibitory synaptic learning rules in this regard *in vivo* would be very hard to obtain and do not currently exist.

Relationship to the literature

We studied the plasticity-driven emerging functional roles for synaptic inhibition and synaptic excitation when there was no *a priori* constraint on their connectivity or what their learning should focus on ('cost function' or 'error signal'). The neurocomputation literature instead often isolates excitatory from inhibitory synaptic plasticity during the learning process or considers inhibitory synapse learning as a homeostatic reaction to the learning in the excitatory synapses (40, 41, 42, 43, 44, 45, 46). It is common practice to regard the inhibition as having a specific

role, such as feed-forward, feedback or blanket inhibition. More selective inhibition has also been modeled (47), in which case it could contribute to subsets of neurons conducting more independent computations (48, 12, 49, 50). But in recurrent networks, it is hard to see how functionally 'clean' roles of inhibition could exist (Fig. 8A). A ground truth here could be that the division into excitatory and inhibitory neurons leads to that the inhibition can act to subtract aspects of the information (sensory or network-internal) that the network already 'knows' hence leaving 'unknown' information to be processed by other neurons in the network (Fig. 8B), both at the 'global' and at a more 'detailed' level, to use a proposed terminology (40).

Here, learning was a consequence of that the spatiotemporal force inputs within the network became a product of their transformations through the tissue and the network internal dynamics. The latter appeared in turn to be a product of the contributions of all synapse types (Fig. S18), i.e. a consequence of the integrated network system. We do not claim that this is the best possible way to learn, only that these are the emergent effects we obtain under these biological-like conditions with relatively few *a priori* constraints and in particular no specific imposed learning goals. The performance of recursive networks are notoriously difficult to quantify in terms of the types of meta-analyses that has been developed for feed-forward networks (51, 52), due to their partially chaotic nature (12), a consequence of their intrinsic complexity. We are not aware of any such meta-analysis for measuring the functionality of fully recursive networks receiving high-dimensional inputs with intrinsic dependencies. Instead, it is common practice in the application of recursive networks, including ESNs, liquid state machines (LiqSM) or RC networks, to simply randomize the internal synaptic weights of the network until a supervisor judges that some useful dynamic behavior emerges (19, 53) and learning is typically limited to the output connections outside this recursive network (13, 19, 53). .

Limitations

We aimed to keep the network as small and generic as possible, to facilitate interpretations of big picture functional effects, and to avoid assumptions regarding connectivity. But this naturally prevented us from exploring the potential variations in the dynamic behavior in specific network configurations without full connectivity. Also, beyond the general functional principle that emerged and that is in agreement with various biological data, at a detailed level we cannot validate our emergent effects using biological data, because there is no neurophysiological analysis available that can provide the required information on both single-neuron connectivity and the electrophysiological dynamic activity patterns across larger populations of cortical neurons. Other limitations were that we only used a set of sensors from a small, uniform tissue model and lacked a thalamus-like information integration.

However, our ambition here was to provide a conceptual angle on fundamental emergent effects in this type of recursive networks, under this learning strategy that included several features observed in biology, with the hope of inspiring new interpretational frameworks for neuroscience to better understand the principles of brain operation.

Materials and Methods

Network Connectivity

We modelled the activity dynamics of two-layer, fully connected recursive neuronal networks comprising both excitatory neurons (ENs) and inhibitory neurons (INs) (Fig. 1A). In the standard networks, there were five ENs & five

INs in layer 1 and four ENs & four INs in layer 2. Only the ENs and INs in layer 1 received external sensory inputs (see section *Sensory Inputs*) as excitatory synaptic connections, i.e., every EN and IN in layer 1 received 10 sensory inputs as excitatory synapses. The weight distribution of those sensory synapses are indicated under 'Initial Synaptic Weights and Initial Connectivity%' (below)). The networks were without autapses (self-excitatory/inhibitory connections) as they were previously observed to amplify the high-frequency parasitic oscillations within recurrent networks with these neuron specifications (10).

Our general network connectivity architecture was motivated from known features of subnetworks within the cortex. In principle, all cortical neuron types, excitatory as well as inhibitory are potential recipients of both thalamic inputs (54, 55, 56) as well as local and long range intracortical connections (55, 56). Our fully connected network was motivated by that recurrent excitatory loops are a common feature in neocortical circuits (57, 58, 59, 60, 61, 62, 63), that inhibitory interneurons provide lateral inhibition (8, 64, 65, 66) as well as feed-forward inhibition (55, 67), but also make synapses on other inhibitory neurons, thereby also potentially forming recurrent disinhibitory loops (68, 69, 70, 71). Hence, both excitatory and inhibitory synapses can form all-to-all local cortical networks (63) in addition to providing long range intracortical connections (72, 73, 74). Hence, the two-layered network was composed of fully connected excitatory and inhibitory neurons (Fig. 1A) where each excitatory and inhibitory synapse was independently and simultaneously subject to Hebbian-like plasticity, with a BCM-like regulation (8, 75).

The skin sensory inputs were provided to the first layer, to both excitatory and inhibitory neurons. The absence of sensory inputs to the second layer was motivated by that the sensory inputs were provided from a specific patch of skin. For such a circumcised part of the sensory population, not all neurons with sensory input will receive that specific input.

Neuron Model

Our previously published non-spiking linear summation neuron model (LSM) was used to compute the activity of both excitatory and inhibitory neurons. LSM is a compact model that emulates the impact of membrane time constants and conductance-based synaptic integration in biological neurons. It is hence capturing the central characteristics of an H-H conductance-based neuron model (10) where the time-continuous output activity is intended to reflect the mean firing rate of a traditional spiking neuron model. In a biological neuron, due to that its electrical signaling is being driven by opening and closing of conductances (ion channels), the impact that the activation of a given synapse results in does not only depend on its synaptic weight, but also on how many other conductances are open at the same time. The LSM represents two types of such conductances. First those of other synapses active at the same time. Secondly, the static leak conductance, which represents the constitutive leak ion channels that establish and maintain the resting membrane potential and that in the biological neuron therefore needs to be always open. A natural consequence of this conductance-based signaling, just like in the biological neuron, is that the higher the activity of all other synapses (or conductances) on the neuron, the lower the impact of a given synapse with a given weight (i.e., a given conductance). This can help protecting neurons from overexcitation, for example, and thus can contribute to stability in the learning network (10). In the LSM, the membrane potential (A, Eq. 1) of a neuron is given by the summation of weighted (w) input synaptic activity (a), that is normalized by emulated membrane conductances (static leak and dynamic leak). The static leak (k) emulates the leak channels contributing to the resting membrane potential and is scaled by the total number of synaptic inputs (i) to the given neuron ($k = 0.25$

per synapse). The dynamic leak (τ) reflects the rate of leak towards the resting potential, normally limited by the membrane capacitance of the neuron, which was a constant ($\tau = 1/100$). The scaling effects of these membrane constants on the neuron activity under various synaptic input conditions were previously reported in (10). The neuron output activity was thresholded at a membrane potential corresponding to zero net synaptic input activity in the neuron (Eq. 2). The neuron activity of LSM is given by Eq. 1 & 2.

$$\tau \frac{dA}{dt} = \frac{\sum(w_i.a_i)}{k + \sum |w_i.a_i|} \tag{1}$$

$$if A < 0, then A = 0 \tag{2}$$

Sensory Inputs

Skin Model

We used a mass-spring-damper model of a slab of skin (Fig. 1B) to generate the sensory input signals (*skin inputs*). This skin model was previously developed to replicate the dispersive mechanical waves that are elicited in biological skin during tactile interaction (2). The spreading mechanical waves, also studied in other experiments (76, 77, 78) create differential skin tissue movements, hence generating shear forces (79, 2), that are known to activate the skin mechanosensors. The masses (circles, Fig. 1B) in this skin model were arranged in three layers, superficially resembling the structural properties of human skin (epidermis, dermis and subcutaneous tissues). The masses were homogeneously distributed in a mesh-grid-like structure along each layer, and in pyramidal structures across layers (color coded as per layer, Fig. 1B). The neighbouring masses were interconnected via a network of springs and dampers (lines, Fig. 1B). In this study the skin model has a mesh size of 20×20 masses in layer 1 (400 masses), 19×19 masses in layer 2 (361 masses) and 18×18 masses in layer 3 (324 masses); interconnected with a 5770 springs and dampers. The model uses the inter-node distance, which is a representation of strain, corresponding to the spring load, as the best available proxy for representing the signal that would drive the activation of mechanoreceptors. The masses on the edges of the skin model (empty circles, Fig. 1B) were fixed in all three axes. To compute the numerical integration, the equation of motion (Eq. 3) for multiple degree-of-freedom spring-mass-damper system can be written in state-space form as in equation 4 (80, 2)

$$M\ddot{q} + C\dot{q} + Kq = f \tag{3}$$

Where M, C and K are matrices denoting mass, stiffness and damping of the whole system and f is the input force vector. q, $\dot{q}$ and $\ddot{q}$ are denoting position, velocity and acceleration of the system respectively.

$$\dot{x}(t) = Ax(t) + Bu(t) \tag{4}$$

Where x is the state vector, u is the applied input force, A is the state matrix, and B is the input matrix. Coupling equation 3 and 4, we obtain

$$M\ddot{q}(t) = -C\dot{q}(t) - Kq(t) + f(t) \tag{5}$$

Which can be written as,

$$\ddot{q}(t) = \begin{bmatrix} 0 & I \\ -M^{-1}K & -M^{-1}C \end{bmatrix} x(t) + \begin{bmatrix} 0 \\ M^{-1} \end{bmatrix} f(t) \tag{6}$$

To compute the numerical solution of the above-described state equation we used an *ode45* solver (fifth order Runge-Kutta method) in MATLAB, with a time step of 0.01 ms. Each mass within the skin model moved freely in the three-dimensional space, the matrices and vectors in the above defined state equation were adapted accordingly. The values of $M, K\&C$ are $1.0\,\mathrm{mg},\ 2.5\,\mathrm{N\,m^{-1}}$ & 5x$10^{-4}\mathrm{N\,s\,m^{-1}}$, as studied in (2).

Skin Inputs

To activate the skin sensors, we designed different spatial skin force patterns that were activated by defining the input force vector (f) of equation 6 as a Gaussian function with a sigma of $1ms$ (Fig 1B, insert). The force vector was three dimensional ($f = [f_x f_y f_z]$), describing the input force across all three axis of the skin. The obtained force across each spring was used as the as the output signals of the skin model, used to drive the activity of the neuronal network (*Skin Input*, Fig. 1C). The forces were given by Hooke's law ($F_s = kx$), where k is the stiffness constant of the spring and x is the rate of change in the position from equilibrium. Out of the 5770 springs available in this skin model, we used only the ten springs connected to the mass in the center of layer 1 (black mass, Fig. 1B). The responses of these ten springs were used for training and testing the networks. The activity of all skin sensor signals were made to be positive-only by rectification of the spring tension signal.

Gaussian Input

As a comparison for the networks that learned from skin model inputs, which have systematic intrinsic dependencies or sensor population regularities across all inputs, we also let some networks learn from 'Gaussian inputs' that lacked such intrinsic dependencies. For each of the 10 Gaussian 'sensors', we used pseudo-random spike trains with a spiking frequency of 1-3 Hz frequency drawn from a normal distribution and convoluted using a Gaussian function to obtain a time-continuous sensory input (*Gaussian Input*, Fig. 1C). An inbuilt MATLAB function "*randi*" was used to generate the spike time distributions and "*gaussmf*" was used for the convolution of the spikes into time-continuous responses. The distribution and convolution parameters for generating the Gaussian activity were chosen to match the power and frequency components of the skin inputs (Fig. S2).

Network Training

For learning we provided the network (Fig. 1A) with a series of 1160 stimulus presentations, either sensory inputs from the skin model or from the Gaussian model (Fig. 1C). A network that learnt from the skin inputs is referred as "*skin network*" and a network that learnt from the Gaussian inputs is referred as "*Gaussian network*". For the skin networks, we used 50 unique skin activation conditions, consisting of five different input types (*indent, push, pull, slide, point push,* Fig. S1) at ten different locations on the surface of the skin model. The 50 different inputs were provided in a predefined (pseudo-)random order. For the Gaussian networks, we generated non-repetitive random activity patterns across the 10 sensors. For both skin and Gaussian training inputs, individual stimulations were applied in a pseudo-random order, at an interval of 3000 ms, for a total of 1160 repetitions, and a total of less than 1 hour of training.

Initial Synaptic Weights and Initial Connectivity%

All the initial synaptic connections ("*initial weights*") in the network were given a weight between 0.001 and 1 (*initial weights*). No weight could ever exceed 1. As all our networks were fully connected no synapse had 0 weight. The initial weights of the whole population of synapses in the network were generated as log-normal distributions with different mean weights (μ) (values between 0.05 to 0.5) and coefficient of variation (σ_{cv}) (values between 10% - 50%). The variance of the distribution was quantified as (σ) = $(\sigma_{cv}/100) * \mu$ (Fig. S11). 'Initial connectivity%' indicated the mean weight in the network but was also a label we used to indicate the different initial weight distribution parameters (μ and σ_{cv}) (Fig. S12). Within each given parameter combination (initial connectivity%) weights were also randomized to obtain five different versions of each initial connectivity% network, which were used to obtain the variances indicated in Figs 4-6.

Synaptic Learning

We used the same Hebbian-inspired '*activity dependent synaptic plasticity rule*' (8) for learning synaptic weights in both excitatory and inhibitory synapses. The learning rule was formulated to reward the correlation between the individual synaptic activity (a_i) and the neuron activity (A). A positive correlation between the neuron & the synaptic activity leads to potentiation (increase) in synaptic weight and decorrelation between these activities leads to depression (decrease) in synaptic weight. For each stimulus presentation ($t_0 - t_n$), the weight change (Δw) of a synapse (i) was given by equation 7.

$$\Delta w_i = \int_{t_0}^{t_n} \{(A(t) - Th) * a_i(t)\} \ . \eta \, . \, \xi \tag{7}$$

The value of the integral ($t_n = 1000ms$) determined the magnitude of the individual synaptic weight changes.

To obtain long-term network stability, we also implemented a regulation of the synaptic plasticity that is related to the BCM rule, using a *learning polarity threshold (Th)*. The learning polarity threshold implements an effect that is related to the BCM rule and defines above what activity level the neuron becomes more likely to depress its afferent synapses, and vice versa (81, 8, 82). The Th was given by equation 8. In this case, we did implement a minor difference between the excitatory and the inhibitory synapses, which led to that the learning polarity threshold was lower for the inhibitory synapses at each given activity level of the postsynaptic neurons (Fig. S19C). This means that the probability of potentiation in the inhibitory synapses was higher for each given neuron activity level, although to a decreasing degree as the neuron activity increased. In particular at low-levels of neuron activity, such as in early stages of learning, this non-linearity enhanced the propagation of excitatory activity through the network.

$$Th = -logn(\mu, \sigma) + A(t) + A_o \tag{8}$$

The strength of potentiation/depression of an individual synaptic weight was also regulated by a learning rate (η) and a compensation factor (ξ). The learning rate was defined as an exponential decay function ($e^{-3.5}$) of the current neuron activity, limiting the rate at which synaptic weight changes occurred (Fig. S19A). The compensation factor constant is given by a sigmoid function (midpoint of 0.5 and steepness of 0.05, Fig. S19B) of current synaptic weight w_i. The compensation factor allowed the weight change of a given synapses to become higher if its current weight was low and vice versa. This factor is motivated by that the insertion of a synaptic receptor in the synaptic

membrane can be regarded as a chemical reaction (the insertion and removal of synaptic receptors is handled by partly separate chemical reactions (83)), where the addition of a new channel will become less likely the higher the number of ion channels already inserted and vice versa (10). The compensation factor function was flipped for depression and potentiation of a synapse (Fig. S19B). The weight change (Δw_i) and learning polarity threshold (*Th*) were computed as moving averages across 100 stimulus presentations in order to dampen their rates of adaptation.

Excitatory Synapse Learning Signal Filter

In general, the excitatory and inhibitory synapses learned using the same Hebbian-like learning rule, based on their activity correlation with the postsynaptic neuron. But for the densest network, this proved to not work as well as for the less densely connected networks, and we therefore implemented a tweak where the excitatory synapse learning was instead based on correlation with a high-pass filtered version of the postsynaptic neuron activity. The purpose was to make the excitatory synapse learning more selective, i.e. it would only correlate with positive changes in the postsynaptic activity. This could for example equal that the the postsynaptic activity in the dendritic spine, or the synaptic subspace underneath the excitatory synapse, would only be exposed to or only react to positive *changes* in the calcium activity of the main compartment of the neuron. Biological studies indicate that the near-synaptic calcium concentration can have different time constants than the calcium concentration in the main compartment of the neuron (84, 85, 86) and specific dynamics in the calcium concentration could impact synaptic plasticity (81). In order to achieve a high-pass filtered version of the postsynaptic activity (A), with which the excitatory synapse activity was correlated to obtain a net weight change, we multiplied that activity with an exponential function (e^x) (Fig. 5C) with different order *x*. This filter was applied only on excitatory synaptic activity (a_i) during the learning phase, in the analysis of Figures 5C,D, S16, S17.

Network Performance (Post-learning)

To evaluate the learning performance, we compared the generalization and the robustness capabilities of the skin networks and the Gaussian networks (Fig. 3). In order to test the generalization, we quantified the classification accuracy across five naive skin stimuli (Fig. S1F - J) or 11 force impulse skin stimuli (Fig. S3), neither of which were used during the learning process (Fig. 3D, F). These inputs were in this testing phase applied to the central mass only (Fig. 1). In order to test the robustness we quantified the classification accuracy across the naive and force impulse input, by randomly removing two sensor input synapses, corresponding to 20% of the total sensor input to the network.

The classification performance was quantified for four noise levels, where random noise of a given signal-to-noise ratio (snr) was added to the activity of each neuron. For each network configuration tested, we reported the average classification performance across the test inputs with 5 different repetitions of each noise level (Fig. 3,4,5).

Statistical Analysis

Total Weight change

Total weight change (ΔW) within a neuron is defined as the summed difference between all the initial weights (W_i^I, pre-learning) and their respective end-weights (W_i^E, post-learning) as given by equation 9. Where, m is total

number of neurons (j) and n is total number of synaptic weights (i) for a given neuron. The average synaptic weight changes across all the neurons was reported in Fig. 4F-I, S14, S15, S17.

$$\Delta W = \frac{1}{m}\sum_{j=1}^{m}\left(\sum_{i=1}^{n}\left(\mathrm{W}_i^E - \mathrm{W}_i^I\right)\right) \tag{9}$$

Cross-correlation

The correlation index measure was used to compute the similarity in the neuronal activities during test inputs. The correlation between two neurons was computed with an inbuilt MATLAB function "*xcorr*" (with zero lag), which produces values from 0 (uncorrelated) to 1 (identical). This pairwise cross correlation was calculated across all neuron pairs and the average value was reported (Fig. 5A-B, S18, S16).

Frequency analysis

A continuous wavelet transform (using an inbuilt MATLAB function "*cwt*") was performed in order to define the frequency composition of the input sensory responses over time. The wavelet transform was used to extract the power of each frequency band as a function of time for the time-continuous responses of the sensors. Here, we reported (Fig. S2), for each frequency band, the maximum power of each sensor across ≈ 1160 stimulus presentations.

Principal component analysis (PCA)

Principal component analysis was performed on the actvitiy of the excitatory neurons using an inbuilt MATLAB function *pca*. The pca function projects the neuron activity onto principal component space (new set of variables, Principal Components (PCs)) that explain the high dimensional input data on fewer output dimensions while encompassing the maximum preservation of information in the input data. The product between the neuron activity and PC coefficients results in "*PC scores*" that represent the sensory signals in PC space (Fig. 3C, E).

Classification

To quantify the classification accuracy across different skin inputs (Fig. 3D, F) we used a linear tree classifier. The excitatory neuron population activity for each given skin input at each defined level of network noise was projected onto the first PC and the PC scores (see section above) were used as input observations to the classifier. Each skin input was repeated for 50 times, where the neuronal noise resulted in different responses for each repetition. The data to the classifier was binned into 5 classes while testing the 5 naive skin inputs (50 repetitions x 5 classes = 250 observations), and 11 classes while testing the 11 force impulse inputs (50 repetitions x 11 classes = 550 observations). As each response consisted of 3000 time steps, the classifier had 3000 predictors for each observation. The classifier was trained and tested using a 5-fold cross-validation, which was repeated for 100 iterations to ensure robustness. This analysis was performed using a Matlab toolbox "*Classification Learner*".

Data Availability

The full set of simulation data used to produce all of the results in this paper is available from the authors upon reviewers request and at publication.

Acknowledgements

This work was funded by EU H2020 FET Open project no. 829186 'ph-coding'.

Competing interests

The authors declare no competing interests.

References

[1] Zador, A. et al. Catalyzing next-generation artificial intelligence through neuroai. Nature communications **14**, 1597 (2023).

[2] Rongala, U. B., Seyfarth, A., Hayward, V. & Jörntell, H. The import of skin tissue dynamics in tactile sensing. Cell Reports Physical Science (2024).

[3] Seyfarth, A., Zhao, G. & Jörntell, H. Whole body coordination for self-assistance in locomotion. Frontiers in Neurorobotics **16**, 883641 (2022).

[4] Heylighen, F. The growth of structural and functional complexity during evolution. The evolution of complexity **8**, 17–44 (1999).

[5] Hayward, V. Is there a 'plenhaptic'function? Philosophical Transactions of the Royal Society B: Biological Sciences **366**, 3115–3122 (2011).

[6] Jörntell, H. et al. Segregation of tactile input features in neurons of the cuneate nucleus. Neuron **83**, 1444–1452 (2014).

[7] Spanne, A. & Jörntell, H. Questioning the role of sparse coding in the brain. Trends in neurosciences **38**, 417–427 (2015).

[8] Rongala, U. B. et al. Intracellular dynamics in cuneate nucleus neurons support self-stabilizing learning of generalizable tactile representations. Frontiers in cellular neuroscience **12**, 210 (2018).

[9] Suryanarayana, S. M., Robertson, B., Wallén, P. & Grillner, S. The lamprey pallium provides a blueprint of the mammalian layered cortex. Current Biology **27**, 3264–3277 (2017).

[10] Rongala, U. B., Enander, J. M., Kohler, M., Loeb, G. E. & Jörntell, H. A non-spiking neuron model with dynamic leak to avoid instability in recurrent networks. Frontiers in computational neuroscience **15** (2021).

[11] Mulholland, H. N., Kaschube, M. & Smith, G. B. Self-organization of modular activity in immature cortical networks. Nature communications **15**, 4145 (2024).

[12] Hennequin, G., Vogels, T. P. & Gerstner, W. Optimal control of transient dynamics in balanced networks supports generation of complex movements. Neuron **82**, 1394–1406 (2014).

[13] Hoerzer, G. M., Legenstein, R. & Maass, W. Emergence of complex computational structures from chaotic neural networks through reward-modulated hebbian learning. Cerebral cortex **24**, 677–690 (2014).

[14] Dean, P., Porrill, J., Ekerot, C.-F. & Jörntell, H. The cerebellar microcircuit as an adaptive filter: experimental and computational evidence. Nature Reviews Neuroscience **11**, 30–43 (2010).

[15] Gibson, E. J. Exploratory behavior in the development of perceiving, acting, and the acquiring of knowledge. Annual review of psychology **39**, 1–42 (1988).

[16] Robinson, S. R., Blumberg, M. S., Lane, M. S. & Kreber, L. S. Spontaneous motor activity in fetal and infant rats is organized into discrete multilimb bouts. Behavioral neuroscience **114**, 328 (2000).

[17] Blumberg, M. S., Marques, H. G. & Iida, F. Twitching in sensorimotor development from sleeping rats to robots. Current Biology **23**, R532–R537 (2013).

[18] Norrlid, J., Enander, J. M., Mogensen, H. & Jörntell, H. Multi-structure cortical states deduced from intracellular representations of fixed tactile input patterns. Frontiers in cellular neuroscience **15**, 677568 (2021).

[19] Gauthier, D. J., Bollt, E., Griffith, A. & Barbosa, W. A. Next generation reservoir computing. Nature communications **12**, 1–8 (2021).

[20] Faisal, A. A., Selen, L. P. & Wolpert, D. M. Noise in the nervous system. Nature reviews neuroscience **9**, 292–303 (2008).

[21] Nilsson, M. N. & Jörntell, H. Channel current fluctuations conclusively explain neuronal encoding of internal potential into spike trains. Physical Review E **103**, 022407 (2021).

[22] Wardlaw, J. M., Smith, C. & Dichgans, M. Mechanisms of sporadic cerebral small vessel disease: insights from neuroimaging. The Lancet Neurology **12**, 483–497 (2013).

[23] Enander, J. M. et al. A model for self-organization of sensorimotor function: the spinal monosynaptic loop. Journal of Neurophysiology **127**, 1460–1477 (2022).

[24] Enander, J. M., Loeb, G. E. & Jörntell, H. A model for self-organization of sensorimotor function: spinal interneuronal integration. Journal of Neurophysiology **127**, 1478–1495 (2022).

[25] Etemadi, L., Enander, J. M. & Jörntell, H. Remote cortical perturbation dynamically changes the network solutions to given tactile inputs in neocortical neurons. Iscience **25** (2022).

[26] Kristensen, S. S. & Jörntell, H. Differential encoding of temporally evolving color patterns across nearby v1 neurons. Frontiers in Cellular Neuroscience **17** (2023).

[27] Trägenap, S., Whitney, D. E., Fitzpatrick, D. & Kaschube, M. The developmental emergence of reliable cortical representations. Nature Neuroscience **28**, 394–405 (2025).

[28] Friston, K. The free-energy principle: a rough guide to the brain? Trends in cognitive sciences **13**, 293–301 (2009).

[29] Clark, A. Whatever next? predictive brains, situated agents, and the future of cognitive science. Behavioral and brain sciences **36**, 181–204 (2013).

[30] Calzolari, D., Della Santina, C., Giordano, A. M., Schmidt, A. & Albu-Schäffer, A. Embodying quasi-passive modal trotting and pronking in a sagittal elastic quadruped. IEEE Robotics and Automation Letters **8**, 2285–2292 (2023).

[31] Stella, F., Achkar, M. M., Della Santina, C. & Hughes, J. Synergy-based robotic quadruped leveraging passivity for natural intelligence and behavioural diversity. Nature Machine Intelligence 1–14 (2025).

[32] Loeb, G. E. Optimal isn't good enough. Biological cybernetics **106**, 757–765 (2012).

[33] Szeier, S. & Jörntell, H. Neuronal networks quantified as vector fields. PLoS Complex Systems **2**, e0000047 (2025).

[34] Oddo, C. M. et al. Artificial spatiotemporal touch inputs reveal complementary decoding in neocortical neurons. Scientific reports **7**, 1–17 (2017).

[35] Kristensen, S. S., Kesgin, K. & Jörntell, H. High-dimensional cortical signals reveal rich bimodal and working memory-like representations among s1 neuron populations. Communications Biology **7**, 1043 (2024).

[36] Stringer, C. et al. Spontaneous behaviors drive multidimensional, brainwide activity. Science **364**, eaav7893 (2019).

[37] Stringer, C., Michaelos, M., Tsyboulski, D., Lindo, S. E. & Pachitariu, M. High-precision coding in visual cortex. Cell **184**, 2767–2778 (2021).

[38] Klushyn, A., Kurle, R., Soelch, M., Cseke, B. & van der Smagt, P. Latent matters: Learning deep state-space models. Advances in Neural Information Processing Systems **34**, 10234–10245 (2021).

[39] McKinney, R. A. Excitatory amino acid involvement in dendritic spine formation, maintenance and remodelling. The Journal of physiology **588**, 107–116 (2010).

[40] Hennequin, G., Agnes, E. J. & Vogels, T. P. Inhibitory plasticity: balance, control, and codependence. Annual review of neuroscience **40**, 557–579 (2017).

[41] Mackwood, O., Naumann, L. B. & Sprekeler, H. Learning excitatory-inhibitory neuronal assemblies in recurrent networks. Elife **10**, e59715 (2021).

[42] Vogels, T. P., Sprekeler, H., Zenke, F., Clopath, C. & Gerstner, W. Inhibitory plasticity balances excitation and inhibition in sensory pathways and memory networks. Science **334**, 1569–1573 (2011).

[43] Clopath, C., Vogels, T. P., Froemke, R. C. & Sprekeler, H. Receptive field formation by interacting excitatory and inhibitory synaptic plasticity. BioRxiv **xxx**, 066589 (2016).

[44] Rubin, R., Abbott, L. & Sompolinsky, H. Balanced excitation and inhibition are required for high-capacity, noise-robust neuronal selectivity. Proceedings of the National Academy of Sciences **114**, E9366–E9375 (2017).

[45] Weber, S. N. & Sprekeler, H. Learning place cells, grid cells and invariances with excitatory and inhibitory plasticity. Elife **7**, e34560 (2018).

[46] Asabuki, T. & Clopath, C. Embedding stochastic dynamics of the environment in spontaneous activity by prediction-based plasticity. Elife **13**, RP95243 (2025).

[47] Rupprecht, P. & Friedrich, R. W. Precise synaptic balance in the zebrafish homolog of olfactory cortex. Neuron **100**, 669–683 (2018).

[48] Vogels, T. P. & Abbott, L. Gating multiple signals through detailed balance of excitation and inhibition in spiking networks. Nature neuroscience **12**, 483–491 (2009).

[49] Denève, S. & Machens, C. K. Efficient codes and balanced networks. Nature neuroscience **19**, 375–382 (2016).

[50] Najafi, M., McMenamin, B. W., Simon, J. Z. & Pessoa, L. Overlapping communities reveal rich structure in large-scale brain networks during rest and task conditions. Neuroimage **135**, 92–106 (2016).

[51] Tyulmankov, D., Yang, G. R. & Abbott, L. Meta-learning synaptic plasticity and memory addressing for continual familiarity detection. Neuron **110**, 544–557 (2022).

[52] Gu, S., Mattar, M. G., Tang, H. & Pan, G. Emergence and reconfiguration of modular structure for artificial neural networks during continual familiarity detection. Science Advances **10**, eadm8430 (2024).

[53] Sun, C. et al. A systematic review of echo state networks from design to application. IEEE Transactions on Artificial Intelligence **5**, 23–37 (2022).

[54] Feyerabend, M., Witte, M., Möck, M. & Staiger, J. F. Functional thalamocortical innervation of vip-and sst-expressing gabaergic interneurons in mouse barrel cortex. iScience 112539 (2025).

[55] Swadlow, H. A. Fast-spike interneurons and feedforward inhibition in awake sensory neocortex. Cerebral Cortex **13**, 25–32 (2003).

[56] Wall, N. R. et al. Brain-wide maps of synaptic input to cortical interneurons. Journal of Neuroscience **36**, 4000–4009 (2016).

[57] Binzegger, T., Douglas, R. J. & Martin, K. A. A quantitative map of the circuit of cat primary visual cortex. Journal of Neuroscience **24**, 8441–8453 (2004).

[58] Song, S., Sjöström, P. J., Reigl, M., Nelson, S. & Chklovskii, D. B. Highly nonrandom features of synaptic connectivity in local cortical circuits. PLoS biology **3**, e68 (2005).

[59] Koestinger, G., Martin, K. A. & Rusch, E. S. Translaminar circuits formed by the pyramidal cells in the superficial layers of cat visual cortex. Brain Structure and Function **223**, 1811–1828 (2018).

[60] Kar, K. & DiCarlo, J. J. Fast recurrent processing via ventrolateral prefrontal cortex is needed by the primate ventral stream for robust core visual object recognition. Neuron **109**, 164–176 (2021).

[61] Douglas, R., Koch, C., Mahowald, M. & Martin, K. The role of recurrent excitation in neocortical circuits. In Models of cortical circuits, 251–282 (Springer, 1999).

[62] Kalisman, N., Silberberg, G. & Markram, H. The neocortical microcircuit as a tabula rasa. Proceedings of the National Academy of Sciences **102**, 880–885 (2005).

[63] Binzegger, T., Douglas, R. J. & Martin, K. A. Topology and dynamics of the canonical circuit of cat v1. Neural Networks **22**, 1071–1078 (2009).

[64] Zhu, J. J. & Lo, F.-S. Recurrent inhibitory circuitry in the deep layers of the rabbit superior colliculus. The Journal of Physiology **523**, 731–740 (2000).

[65] Douglas, R. J. & Martin, K. A. Inhibition in cortical circuits. Current biology **19**, R398–R402 (2009).

[66] Obermayer, J. et al. Lateral inhibition by martinotti interneurons is facilitated by cholinergic inputs in human and mouse neocortex. Nature communications **9**, 1–14 (2018).

[67] Isaacson, J. S. & Scanziani, M. How inhibition shapes cortical activity. Neuron **72**, 231–243 (2011).

[68] Jörntell, H. & Ekerot, C.-F. Receptive field plasticity profoundly alters the cutaneous parallel fiber synaptic input to cerebellar interneurons in vivo. Journal of Neuroscience **23**, 9620–9631 (2003).

[69] Pi, H.-J. et al. Cortical interneurons that specialize in disinhibitory control. Nature **503**, 521–524 (2013).

[70] Sultan, K. T. & Shi, S.-H. Generation of diverse cortical inhibitory interneurons. Wiley Interdisciplinary Reviews: Developmental Biology **7**, e306 (2018).

[71] Cardin, J. A. Inhibitory interneurons regulate temporal precision and correlations in cortical circuits. Trends in neurosciences **41**, 689–700 (2018).

[72] Hafner, G. et al. Mapping brain-wide afferent inputs of parvalbumin-expressing gabaergic neurons in barrel cortex reveals local and long-range circuit motifs. Cell reports **28**, 3450–3461 (2019).

[73] Luo, P. et al. Whole brain mapping of long-range direct input to glutamatergic and gabaergic neurons in motor cortex. Frontiers in neuroanatomy **13**, 44 (2019).

[74] Ährlund-Richter, S. et al. A whole-brain atlas of monosynaptic input targeting four different cell types in the medial prefrontal cortex of the mouse. Nature neuroscience **22**, 657–668 (2019).

[75] Kohler, M., Röhrbein, F., Knoll, A., Albu-Schäffer, A. & Jörntell, H. The bcm rule allows a spinal cord model to learn rhythmic movements. Biological Cybernetics **117**, 275–284 (2023).

[76] Wiertlewski, M. & Hayward, V. Mechanical behavior of the fingertip in the range of frequencies and displacements relevant to touch. Journal of biomechanics **45**, 1869–1874 (2012).

[77] Shao, Y., Hayward, V. & Visell, Y. Spatial patterns of cutaneous vibration during whole-hand haptic interactions. Proceedings of the National Academy of Sciences **113**, 4188–4193 (2016).

[78] Shao, Y., Hayward, V. & Visell, Y. Compression of dynamic tactile information in the human hand. Science Advances **6**, eaaz1158 (2020).

[79] Hayward, V. et al. Spatio-temporal skin strain distributions evoke low variability spike responses in cuneate neurons. Journal of The Royal Society Interface **11**, 20131015 (2014).

[80] Inman, D. J. Vibration with control (John Wiley & Sons, 2017).

[81] Graupner, M. & Brunel, N. Calcium-based plasticity model explains sensitivity of synaptic changes to spike pattern, rate, and dendritic location. Proceedings of the National Academy of Sciences **109**, 3991–3996 (2012).

[82] Rongala, U. B., Mazzoni, A., Spanne, A., Jörntell, H. & Oddo, C. M. Cuneate spiking neural network learning to classify naturalistic texture stimuli under varying sensing conditions. Neural Networks **123**, 273–287 (2020).

[83] Jörntell, H. & Hansel, C. Synaptic memories upside down: bidirectional plasticity at cerebellar parallel fiber-purkinje cell synapses. Neuron **52**, 227–238 (2006).

[84] Wang, S. S.-H., Denk, W. & Häusser, M. Coincidence detection in single dendritic spines mediated by calcium release. Nature neuroscience **3**, 1266–1273 (2000).

[85] Isope, P. & Murphy, T. H. Low threshold calcium currents in rat cerebellar purkinje cell dendritic spines are mediated by t-type calcium channels. The Journal of physiology **562**, 257–269 (2005).

[86] Tigaret, C. M., Olivo, V., Sadowski, J. H., Ashby, M. C. & Mellor, J. R. Coordinated activation of distinct ca2+ sources and metabotropic glutamate receptors encodes hebbian synaptic plasticity. Nature communications **7**, 1–14 (2016).

[87] Yin, P., Esser, E. & Xin, J. Ratio and difference of l_1 and l_2 norms and sparse representation with coherent dictionaries. Communications in Information and Systems **14**, 87–109 (2014).

Acknowledgements

This work was supported by the EU Grant FET 829186 ph-coding (Predictive Haptic COding Devices In Next Generation interfaces), the Swedish Research Council (Project Grant No. K2014-63X-14780-12-3).)

Author Information

Contributions

U.B.R. and H.J., designed and performed the research.

Competing Interests

The authors declare that they have no competing interests.

Correspondence

Correspondence and requests for materials should be addressed to
Udaya B Rongala (email: udaya_bhaskar.rongala@med.lu.se) and Henrik Jörntell (email: henrik.jorntell@med.lu.se)

Supplementary Material

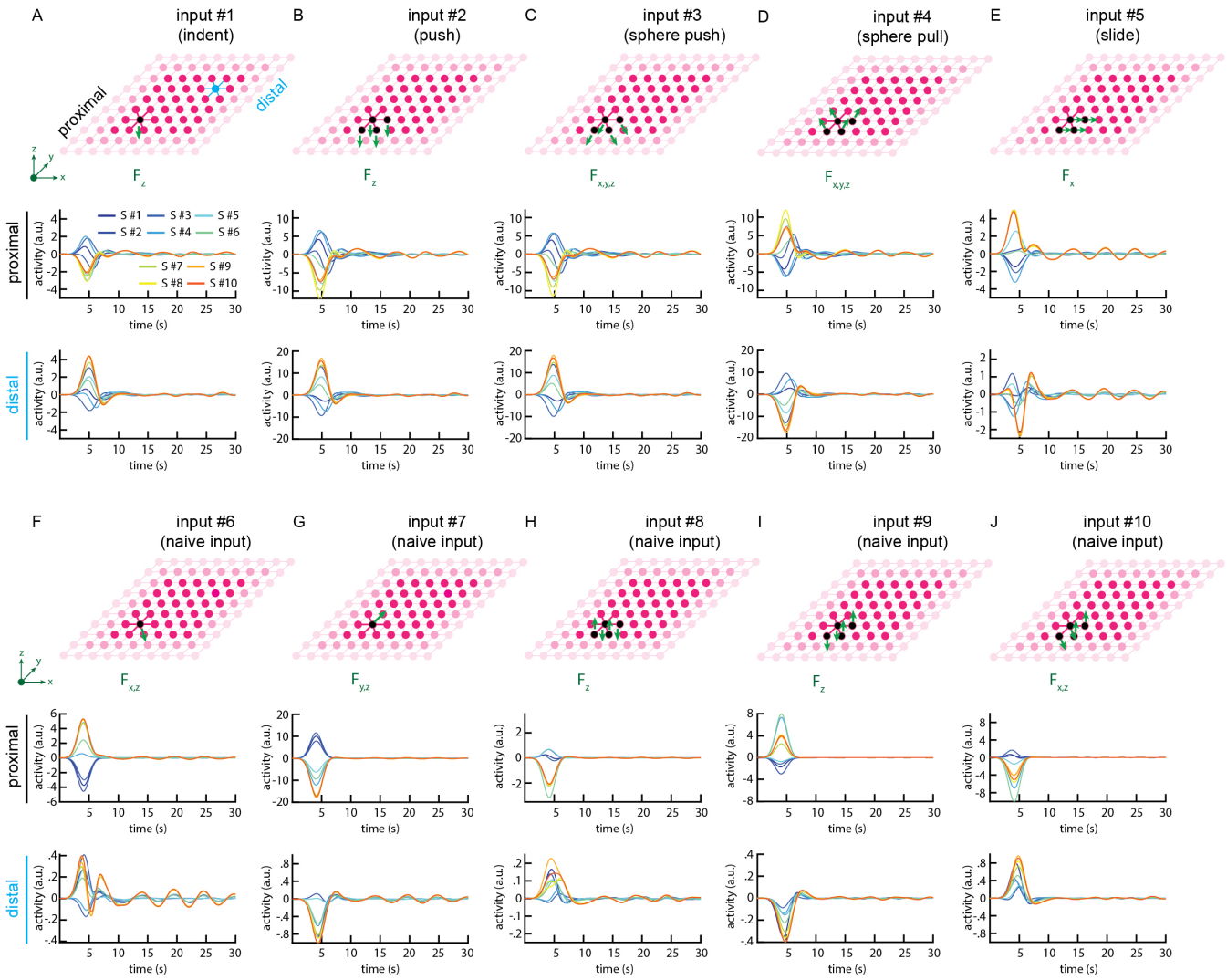

Supplementary Figure 1: Skin sensor responses (spring forces) from the 10 springs attached to the proximal (node colored in black) (used as S#1 - S#10 for the network training) as well as 10 springs attached to a distal node (node colored in blue). The responses of the two population of sensors were shown separately for each input. Note that each input had the same duration but differed with respect to the spatial force distribution along the x-/y-/z-axes ($[f_x f_y f_z]$, as indicated by the green arrows). (**A-E**) The five stimuli used for network learning. (**F-J**) The naive stimuli used for testing generalization capabilities in Fig. 3. Note that the actual skin model was composed of more nodes than illustrated in the display.

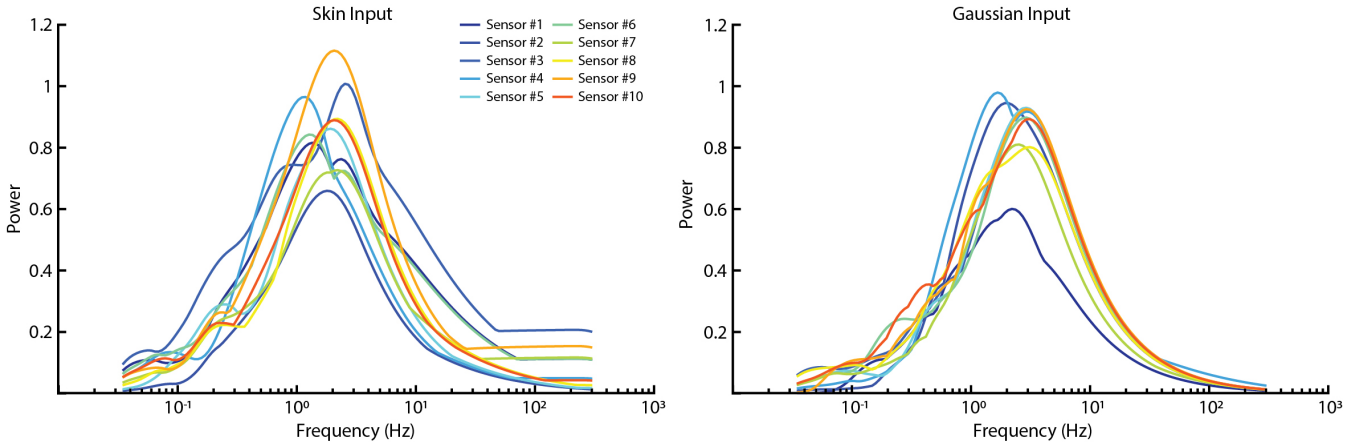

Supplementary Figure 2: Frequency power distribution of all ten skin and Gaussian sensory inputs, averaged across 3500 stimulus presentations.

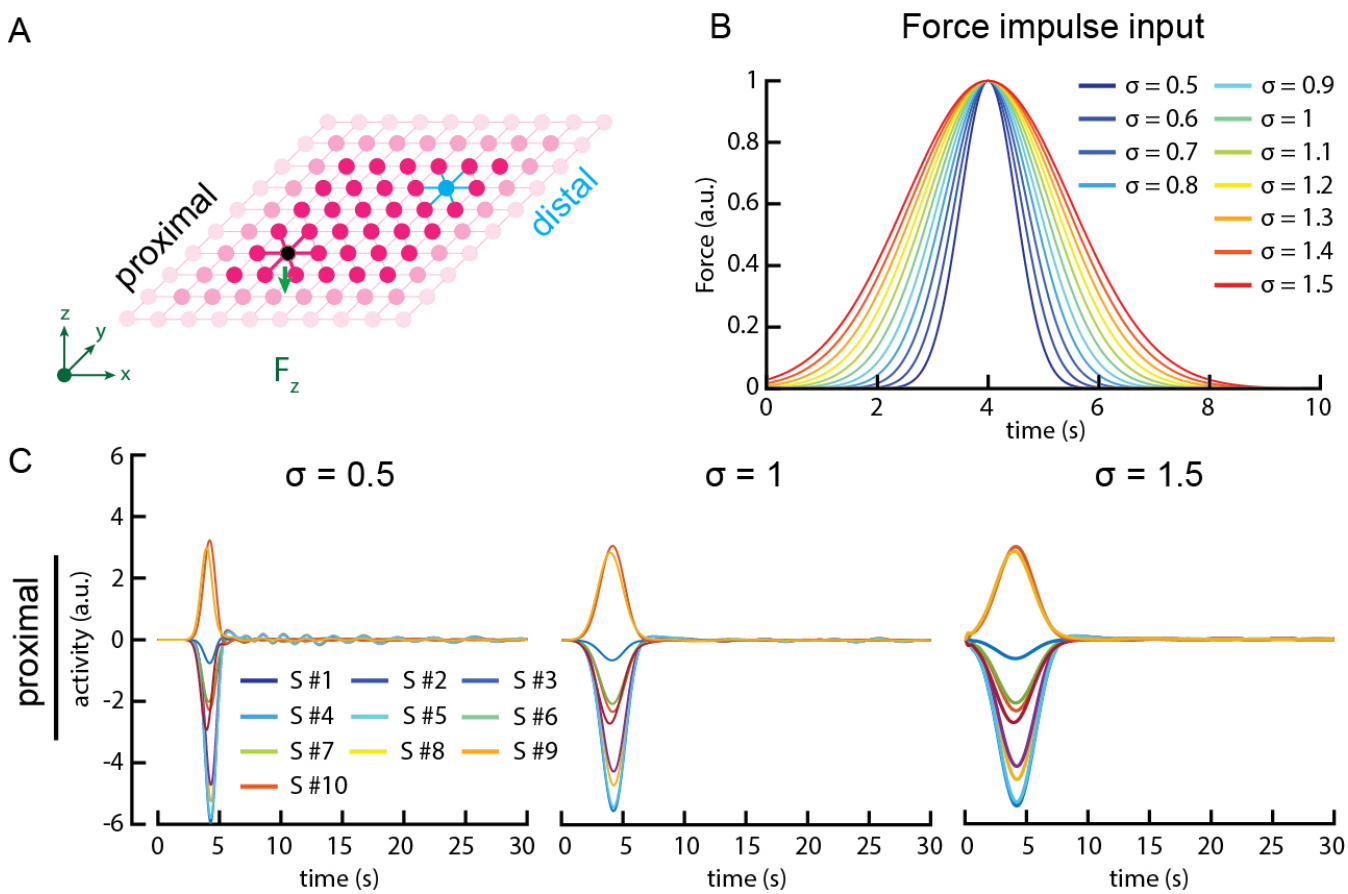

Supplementary Figure 3: The force impulse input consisted of applying a time-evolving force to one mass only. The mass in black was impacted by a force in the z direction (A). (B) The force was applied with a Gaussian function, and force impulses differed solely by the sigma of their temporal Gaussian function. This contrasted with the skin inputs for which the temporal Gaussian function was always the same (σ=1). (C) Example responses of the proximal sensors, i.e. the 10 sensors connected to the proximal mass.

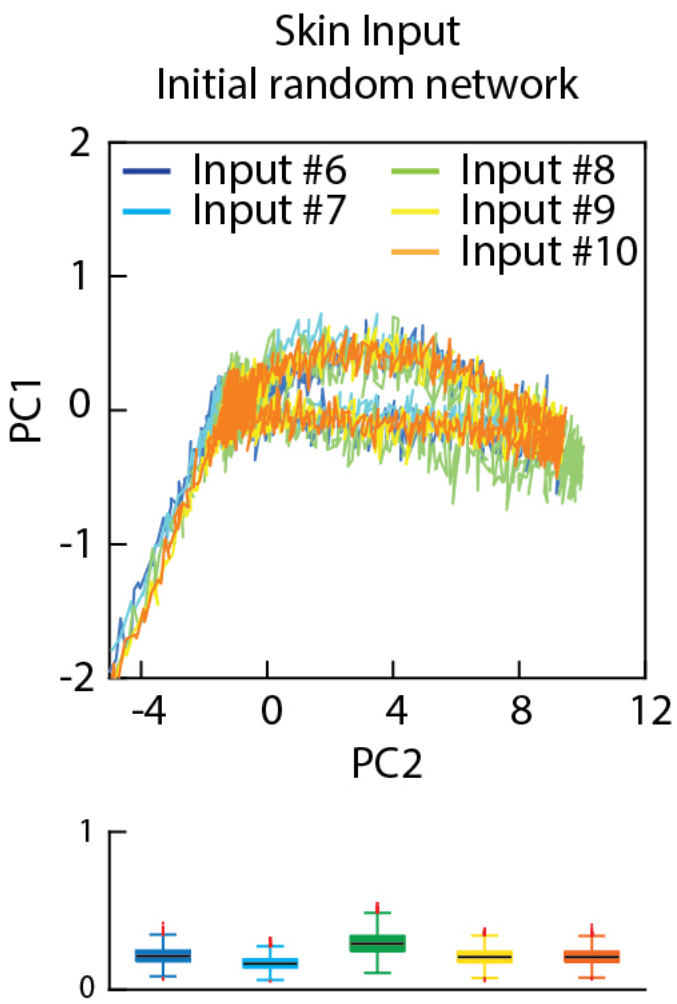

Supplementary Figure 4: **Projection of the neuron population activity from the pre-learning random network onto principal component space.** The output of the neuron population for five different naive skin inputs (Fig. 1F-J) projected on the first two principal components (PCs) (at a neuronal noise level of 0.1, same as in Fig. 3C,E). Inset: the variance of the PCs across the 50 different initial noise randomizations.

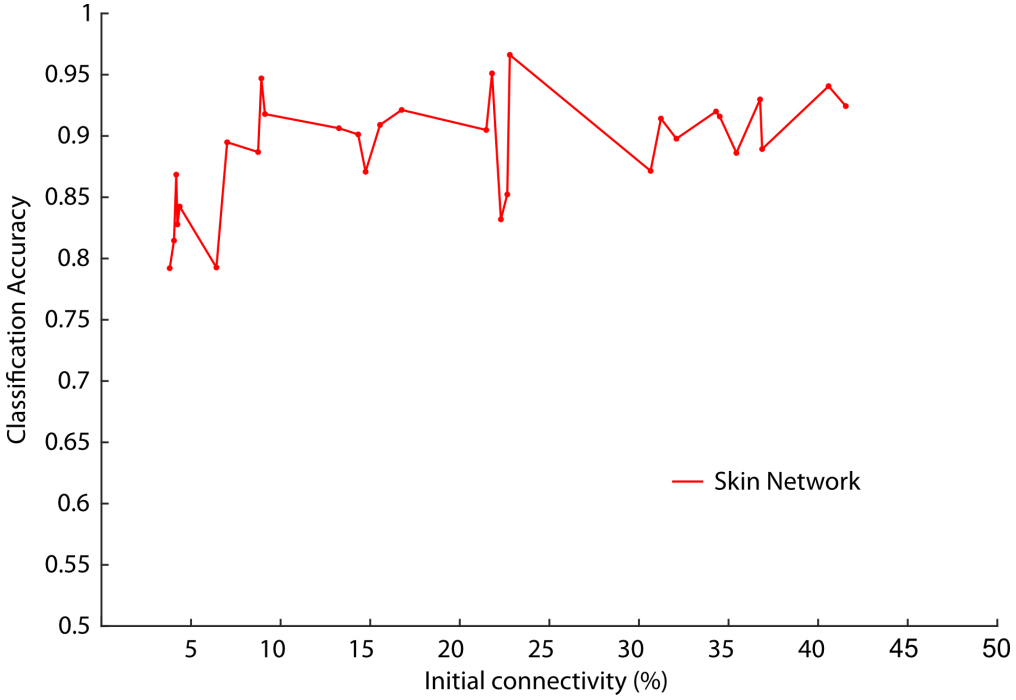

Supplementary Figure 5: Classification accuracy across the five naive skin inputs (similar to Fig. 3) for Skin networks with varied initial connectivity (at a neuronal noise level of 0.1).

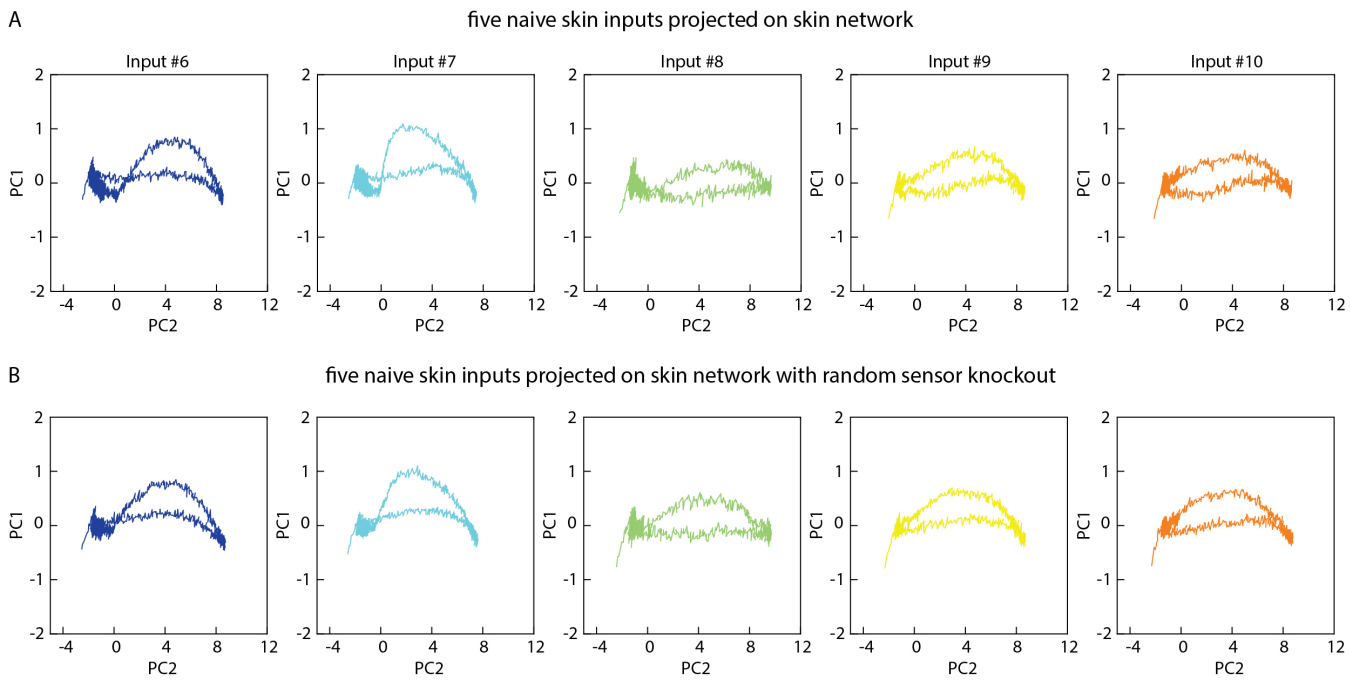

Supplementary Figure 6: **Effect of sensory knockout on the neuron population activity in the skin network.** (**A**) The output of the neuron population for five different naive skin inputs (Fig. 1F-J) projected on the first two principal components (PCs). The plots illustrate outputs for the skin networks (same plots as in Fig. 3C, but here shown separately for each input rather than superimposed). (**B**) Similar display as in **A**, but with 'knock-out' of two random skin sensors post-learning.

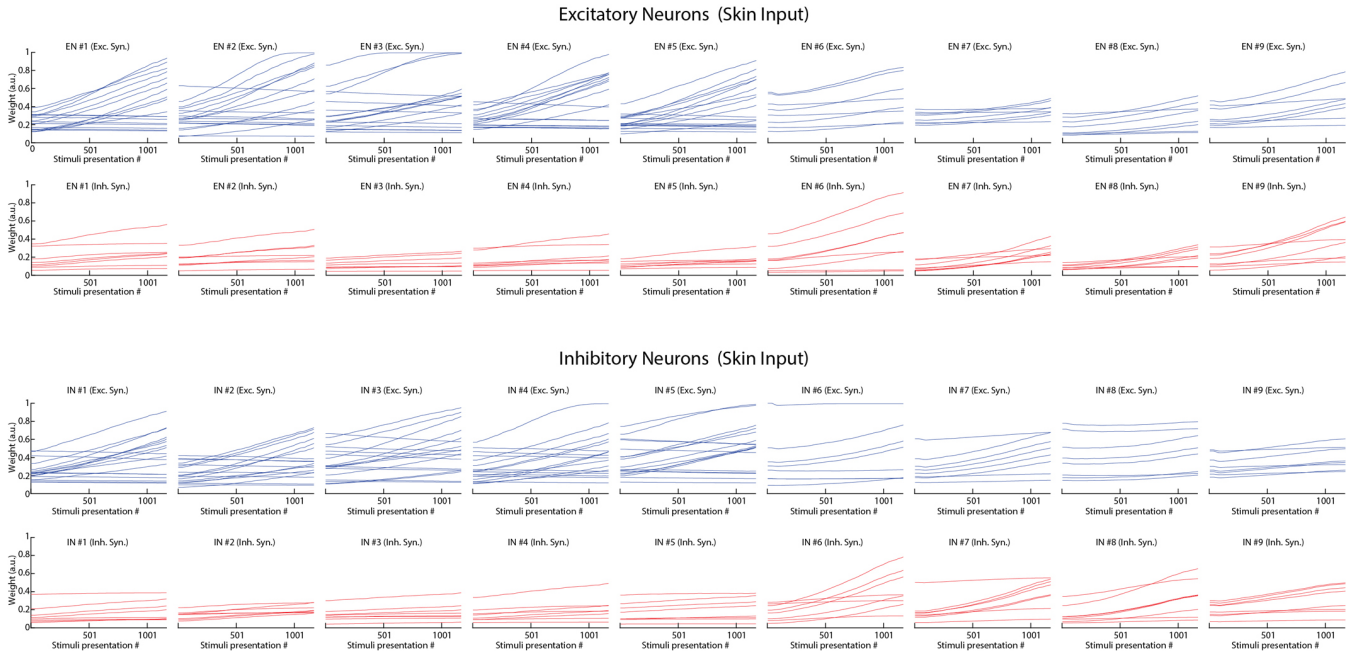

Supplementary Figure 7: Excitatory and inhibitory synaptic weight evolution across all 18 neurons (9 EN & 9 IN) in the network, for learning based on skin inputs. The initial weights (weight distribution at stimulus presentation #1) correspond to the weights matrix in Fig. 4A. The end weights correspond to the weight matrix in Fig. 4B

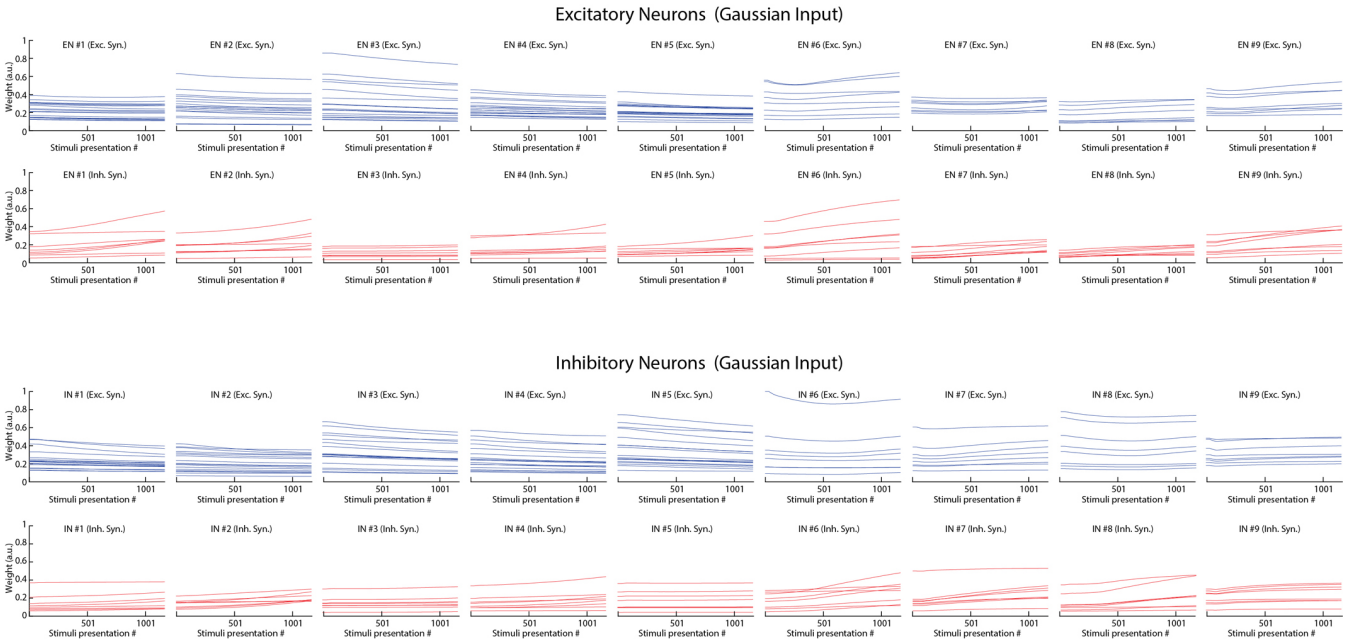

Supplementary Figure 8: Excitatory and inhibitory synaptic weight evolution across all 18 neurons (9 ENs & 9 INs) in the network, for learning based on Gaussian inputs. The initial weights (weight distribution at stimulus presentation #1) correspond to the weights matrix in Fig. 4A. The end weights correspond to the weight matrix in Fig. 4C.

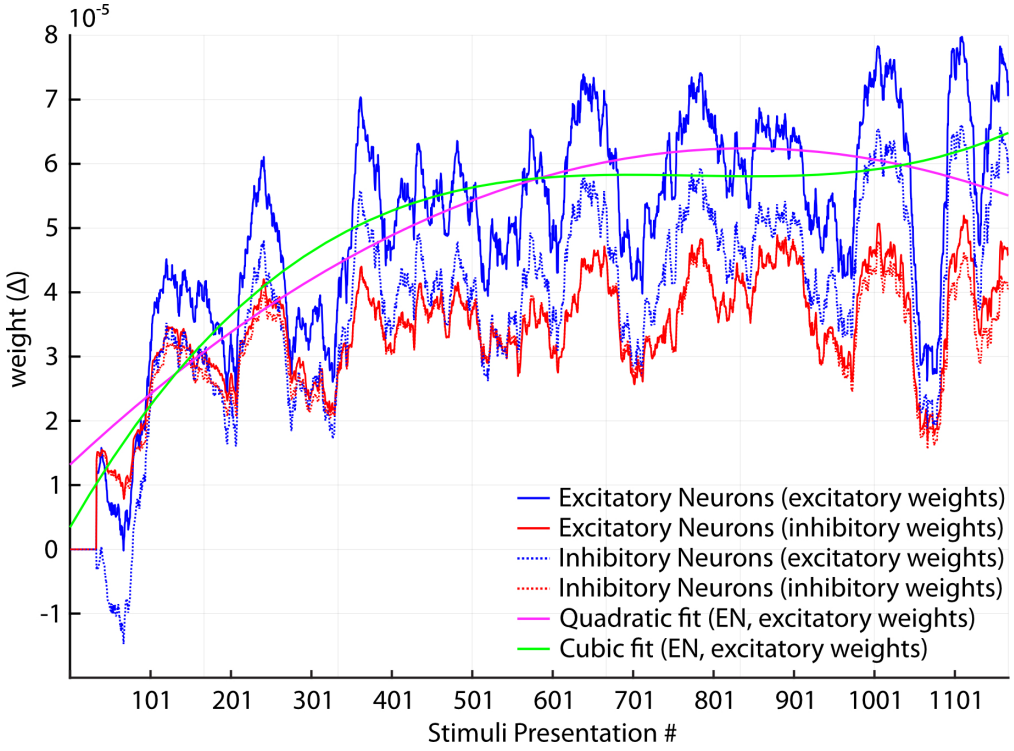

Supplementary Figure 9: Excitatory and inhibitory synaptic weight change for all the stimuli presentation, across all 18 neurons (9 ENs & 9 INs) in the network.

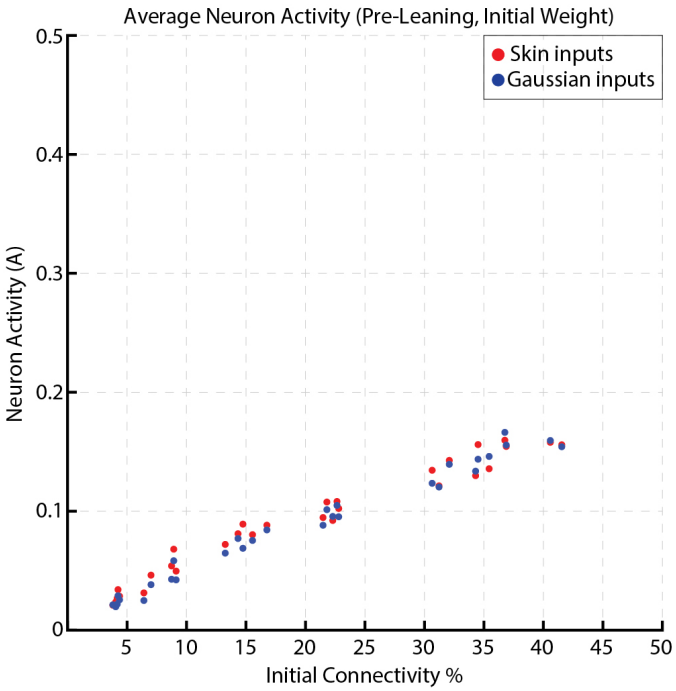

Supplementary Figure 10: The average activity across all the neurons in the network for a given initial weight connectivity % and multiple sensory inputs (skin input & Gaussian input)

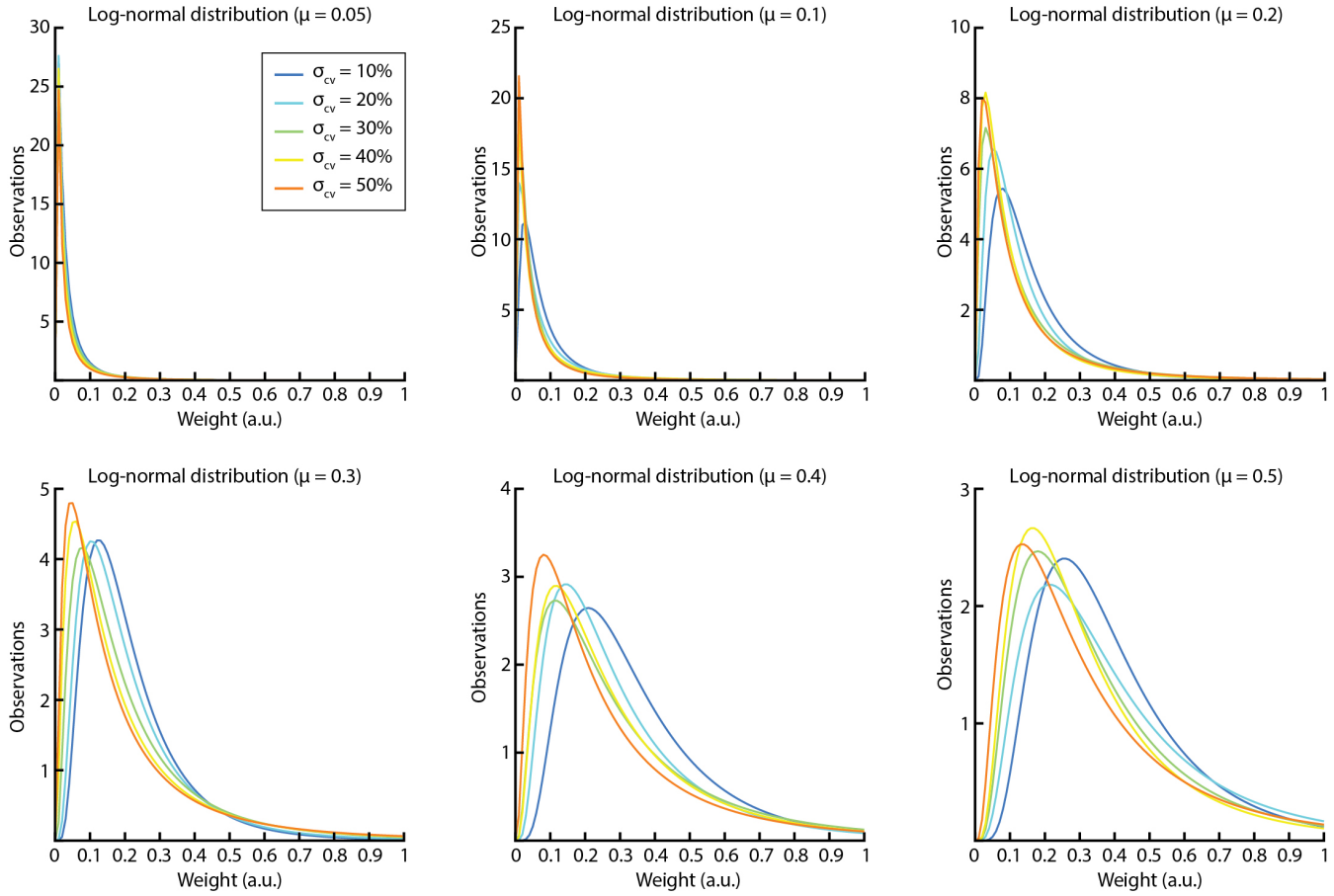

Supplementary Figure 11: The 30 different initial weight settings tested. We used six different mean weights (μ; ranging between 0.05 & 0.5). For each mean weight, we used five different levels of synaptic weight spread, expressed as a the coefficient of variation (σ_{cv}, ranging between 10% & 50%). The variance of the distribution of the initial weights was instead (σ) = $(\sigma_{cv}/100) * \mu$. Each of the 30 different initial weight settings had its own randomization across the synapses, the numbers presented here only illustrates the data at the synaptic population level.

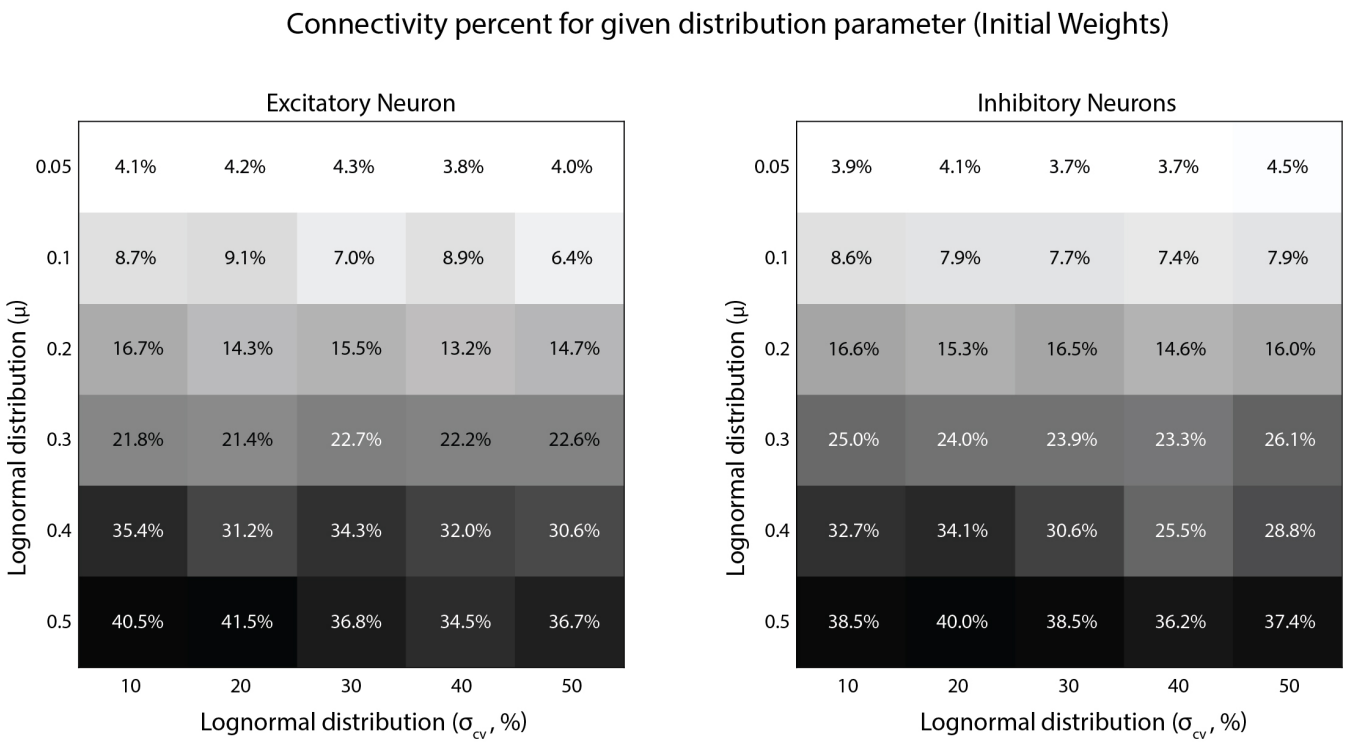

Supplementary Figure 12: Network parameter settings for each specific Initial Connectivity% label. μ and σ_{cv} refers to the distributions in Fig. S11. $Connectivity\% = \sum initial\ weights\ /\ number\ of\ synapses.$

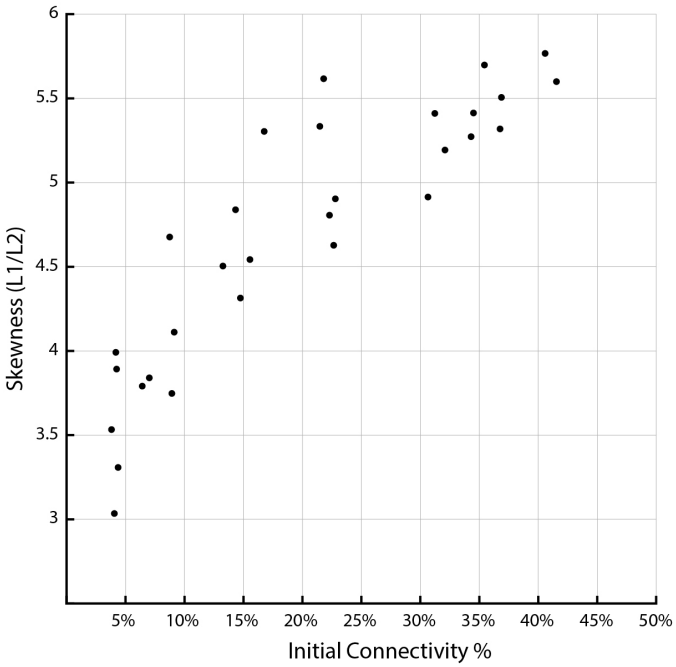

Supplementary Figure 13: The skewness of initial synaptic weight distribution for a given connectivity %. The synaptic weight skewness was calculated as the ratio between the *l1* and *l2* norm of the weight vector (87). This measure will report its minimal value when all synapses have the same weight and a maximum value when one synapse has maximum weight and all other synapses have zero weight.

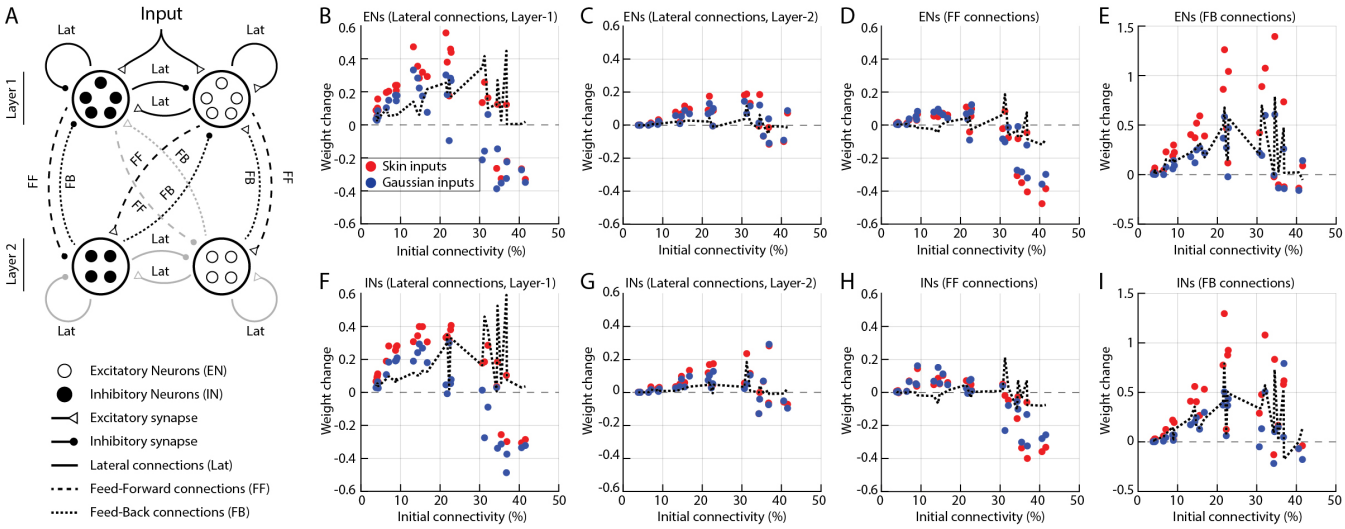

Supplementary Figure 14: **Synaptic weight changes resulting from learning for specific subtypes of synaptic connections.** Same display conventions as in Fig. 4. (**A**) Schematic of the fully connected network structure studied; with specific labels for each type of connection. "*Lat*": Lateral connections within a layer, "*FF*": feed-forward connections from neurons in layer 1 to neurons in layer 2, "*FB*": feed-back connections from neurons in layer 2 to neurons in layer 1. (**B**) Weight changes across all the excitatory and inhibitory lateral synaptic connections on excitatory neurons (*EN*) in layer 1. (**C**) Weight changes across all the lateral synapses on excitatory neurons in layer 2. (**D**) Weight changes across all the feed-forward synapses on excitatory neurons in layer 2. (**E**) Weight changes across all the feedback synapses on excitatory neurons in layer 1. (**F-I**) Weight change analysis similar to that in **B-E**, but instead for synaptic connections made on inhibitory neurons (*IN*). Overall, as in Fig. 4 the weights of all types of synaptic connections tended to increase, up to a certain level of mean initial connectivity (30%), above which the weights instead was decreased by the training. Across all conditions, except for the FF connections the weights increased more with the Skin input than with the Gaussian input (black dashed lines indicates the net difference between the two input conditions).

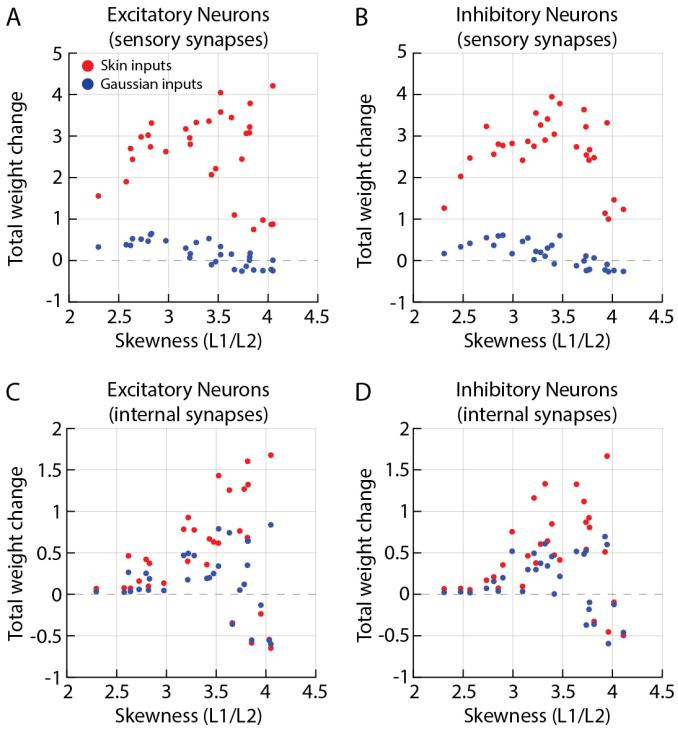

Supplementary Figure 15: **Effects of learning on synaptic weights.** (**A**-**D**) The panels display average weight changes between pre-/post-learning, across all synapses of the indicated category (sensory synapses in **A**, **B** *and* internal synapses in **C**, **D**) for networks with varying skewness of initial synaptic weight distribution (Fig. S13) and sensory input type. Red markers indicate weight change within networks trained on skin inputs and blue markers for corresponding networks trained on Gaussian inputs. (**A**) Weight changes of the sensory synapses on ENs. (**B**) Weight changes of the sensory synapses on INs. (**C**) Weight changes of all excitatory and inhibitory internal synapses on ENs. (**D**) Weight changes of all excitatory and inhibitory internal synapses on INs.

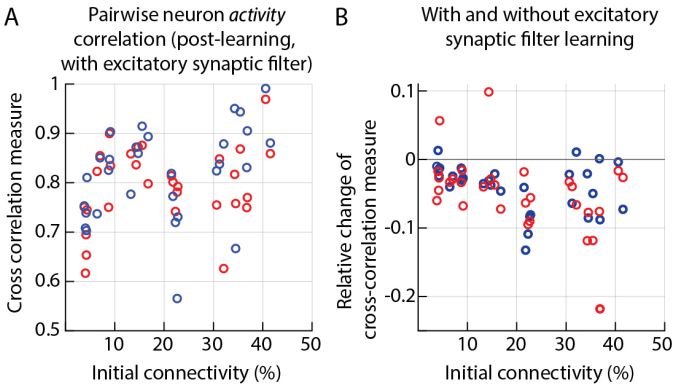

Supplementary Figure 16: **Effect of the excitatory synaptic learning signal filter on the neuronal cross-correlation.**(**A**) Average pairwise cross-correlation measure across all the ENs activity in a network post-learning with excitatory synaptic learning signal filter of $e^{1.4}$ (dotted vertical line in (Fig. 5C)), for networks with different initial connectivity and sensory inputs. (**B**) Net change in the cross-correlation measure of excitatory neuron activity caused by the learning signal filter (difference between (**A**) and Fig. 5B).

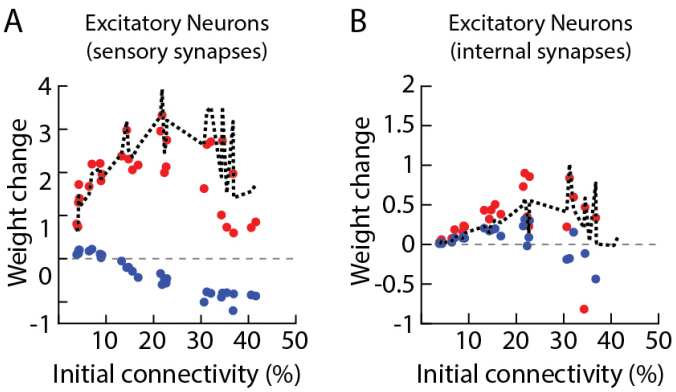

Supplementary Figure 17: **Effect of excitatory synaptic learning signal filter on synaptic weights.** (**A**) Weight change across all the sensory synapses that project as excitatory synaptic connections on excitatory neurons in layer 1 for networks with different initial weight configurations. (**B**) Weight change across all the internal synapses that project as excitatory and inhibitory synaptic connections on all the excitatory neurons within the network. *Note:* **A & B** All networks were trained with the same excitatory synapse learning signal filter of $e^{1.4}$ indicated by the vertical dotted line in Fig. 5B.

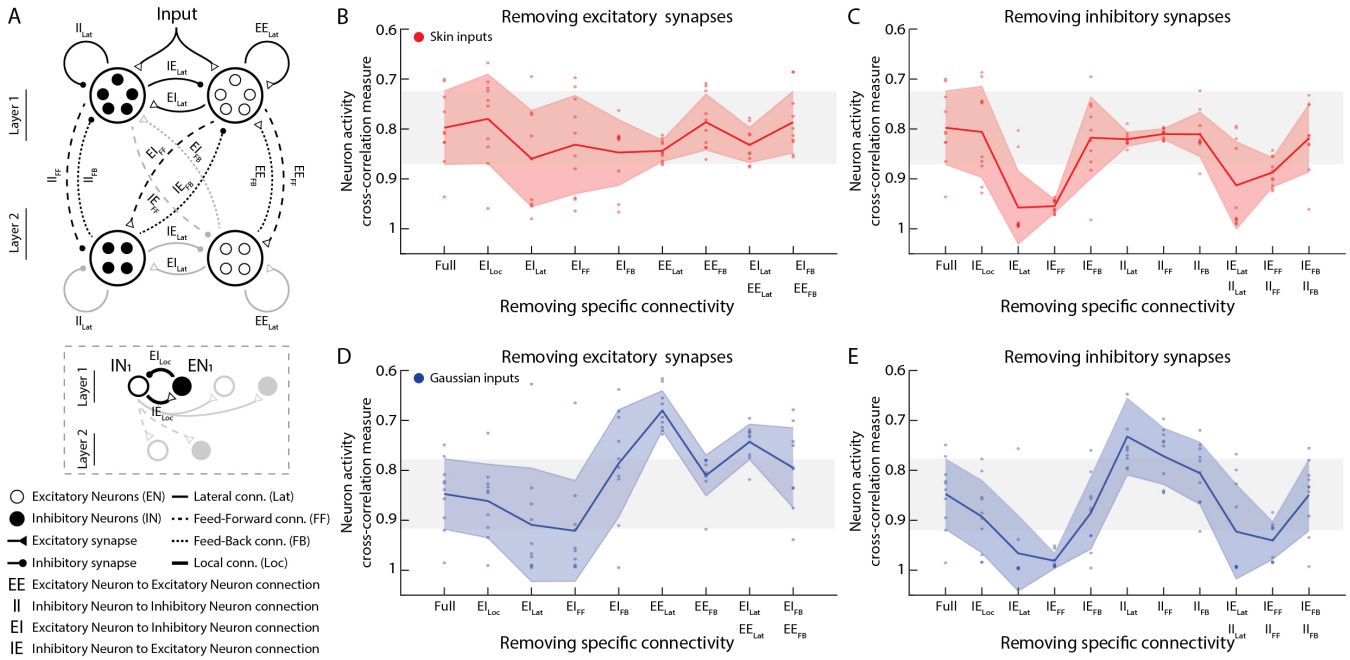

Supplementary Figure 18: **Impact of removing specific synaptic connections on learning quality.** (**A**) Schematic of the fully connected network structure studied; with the insert showing specific labels for the type of individual excitatory and inhibitory synaptic connections between excitatory (ENs) and inhibitory neurons (INs). (**B**) The impact of removing specific types of outgoing excitatory neuron synaptic connections on the learning quality, as indicated by the average pairwise cross correlation measure post-learning. All learning is performed with skin inputs. *Note*: Full connectivity implies that the network has all the excitatory connections intact. The grey zone indicates the range of cross-correlation measures obtained with the Full connectivity. (**C**) The impact of removing specific types of outgoing inhibitory neuron synaptic connections on the learning. *Note*: Full connectivity implies that the network has all inhibitory connections. (**D, E**) Similar to **B, C**, where learning is performed with Gaussian inputs. The excitatory and inhibitory synaptic connections between ENs and INs were labelled as, "***EE***": connections between excitatory - excitatory neurons, "***EI***": connections between excitatory - inhibitory neurons, "***II***": connections between inhibitory - inhibitory neurons, "***IE***": connections between inhibitory - excitatory neurons. The topological connectivity between ENs and INs were labelled as, "***Lat***": Lateral connections withing the ENs and INs in given layers, "***FF***": feed-forward connections from ENs and INs in layer 1 to layer 2, "***FB***": feed-back connections from ENs and INs in layer 2 to layer 1. (*insert*) "***Loc***": Local connections between neighboring ENs and INs (local connection between EN_i and IN_i). The network has initial connectivity of 37% (log-normal distribution, $\mu = 0.5$, $\sigma_{cv} = 10\%$, Fig. S11, S12). Ten different randomized initial weight vectors were generated for the same distribution parameters (individual marker for each given network configuration in **B-E**). All the network configuration learn with an excitatory synaptic filter of $e^{1.4}$(Fig. 5A, dotted line).

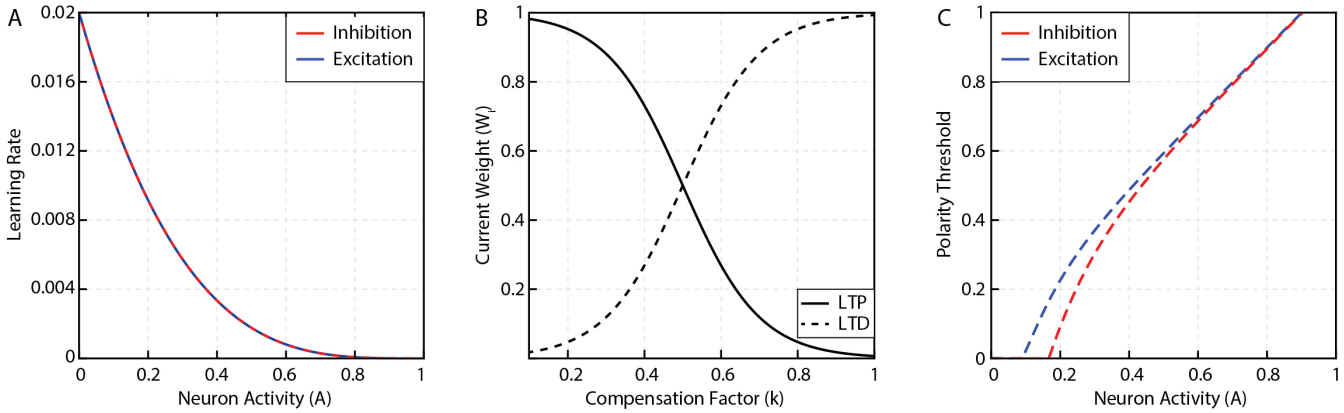

Supplementary Figure 19: Illustration of multiple functions used for synaptic learning process in this study. (**A**) Learning rate as a function of neuron activity (A). (**B**) Compensation factor as function of current synaptic weight (W_i). (**C**) Learning polarity threshold as a function of neuron activity (A).